HHS Public Access

Author manuscript

Sci Signal. Author manuscript; available in PMC 2018 April 17.

Published in final edited form as:

Sci Signal. ; 10(501): . doi:10.1126/scisignal.aaj1784.

The matricellular protein TSP1 promotes human and mouse endothelial cell senescence through CD47 and Nox1

Daniel N. Meijles[1,2,*], **Sanghamitra Sahoo**[1,2], **Imad Al Ghouleh**[1,2,3], **Jefferson H. Amaral**[1,2], **Raquel Bienes-Martinez**[1], **Heather E. Knupp**[1], **Shireen Attaran**[2], **John C. Sembrat**[1,2], **Seyed M. Nouraie**[4], **Mauricio M. Rojas**[1,4], **Enrico M. Novelli**[1], **Mark T. Gladwin**[1,4], **Jeffrey S. Isenberg**[1,2,4], **Eugenia Cifuentes-Pagano**[1,2], and **Patrick J. Pagano**[1,2,†]

[1]Pittsburgh Heart, Lung and Blood Vascular Medicine Institute, University of Pittsburgh, Pittsburgh, PA 15261, USA

[2]Department of Pharmacology and Chemical Biology, University of Pittsburgh, Pittsburgh, PA 15261, USA

[3]Division of Cardiology, Department of Medicine, University of Pittsburgh, Pittsburgh, PA 15261, USA

[4]Division of Pulmonary, Allergy and Critical Care Medicine, Department of Medicine, University of Pittsburgh, Pittsburgh, PA 15213, USA

Abstract

Senescent cells withdraw from the cell cycle and do not proliferate. The prevalence of senescent compared to normally functioning parenchymal cells increases with age, impairing tissue and organ homeostasis. A contentious principle governing this process has been the redox theory of aging. We linked matricellular protein thrombospondin 1 (TSP1) and its receptor CD47 to the activation of NADPH oxidase 1 (Nox1), but not of the other closely related Nox isoforms, and associated oxidative stress, and to senescence in human cells and aged tissue. In human endothelial cells, TSP1 promoted senescence and attenuated cell cycle progression and proliferation. At the molecular level, TSP1 increased Nox1-dependent generation of reactive oxygen species (ROS), leading to the increased abundance of the transcription factor p53. p53 mediated a DNA damage response that led to senescence through Rb and $p21^{cip}$, both of which inhibit cell cycle progression. Nox1 inhibition blocked the ability of TSP1 to increase p53 nuclear localization and $p21^{cip}$ abundance and its ability to promote senescence. Mice lacking TSP1 showed decreases in ROS production, $p21^{cip}$ expression, p53 activity, and aging-induced senescence. Conversely, lung tissue from aging humans displayed increases in the abundance of

†Corresponding author: pagano@pitt.edu.

*Present address: Molecular and Clinical Sciences Research Institute, St. George's University of London, London SW17 0RE, UK.

SUPPLEMENTARY MATERIALS

www.sciencesignaling.org/cgi/content/full/10/501/eaaj1784/DC1

Author contributions: D.N.M. and P.J.P. conceived and designed the experiments. D.N.M., I.A.G., S.S., J.H.A., R.B.-M., H.E.K., S.A., and J.C.S. performed the experiments. D.N.M., I.A.G., S.S., E.C.-P., M.M.R., E.M.N., M.T.G., J.S.I., S.M.N., and P.J.P. analyzed and interpreted the data. D.N.M., P.J.P., E.C.-P., and S.S. drafted the manuscript.

Competing interests: P.J.P. is named on a filed patent (US patent no. 9,187,528 B2) for NoxA1ds. All other authors declare that they have no competing interests.

vascular TSP1, Nox1, p53, and $p21^{cip}$. Finally, genetic ablation or pharmacological blockade of Nox1 in human endothelial cells attenuated TSP1-mediated ROS generation, restored cell cycle progression, and protected against senescence. Together, our results provide insights into the functional interplay between TSP1 and Nox1 in the regulation of endothelial senescence and suggest potential targets for controlling the aging process at the molecular level.

INTRODUCTION

Aging represents a major global health challenge because improvements in disease management prolong life but often at a substantial financial burden (1). Strikingly, worldwide life span elongation and disease comorbidities are strongly associated, a pattern typified in cardiopulmonary-vascular diseases (2). However, specific targeted therapies combating vascular decline in the aging process are absent despite viable regimens to manage vascular diseases (3). Therefore, new mechanistic challenges exist as a consequence of the aging process and an overall decline in holistic health. It is logical, therefore, that attacking the seminal cause of aging rather than individual disease processes will promote greater improvements in life span and quality of life (4).

Cellular senescence is recognized as a central hallmark of the aging process, which occurs when cells withdraw from the cell cycle and lose the capacity to proliferate in response to growth factors or mitogens (5, 6). Moreover, senescent vascular cells are observed in human atherosclerotic plaques and hypertensive samples (7, 8). Senescence is an irreversible form of cell cycle arrest initiated by various stresses including genotoxic and oxidative stress (9), leading to DNA damage, oncogene activation, and telomere shortening (10). Although senescent cells remain minimally functional and metabolically active, they cannot undergo mitosis, and augmented senescence is deleterious to organ function vis-à-vis interference with tissue self-renewal.

In addition to cell cycle arrest, senescent cells accumulate senescence markers, including senescence-associated β-galactosidase (SA-β-Gal), and secrete vasoactive factors (11). Matricellular thrombospondins were initially characterized as a highly abundant family of proteins in Werner syndrome fibroblasts, which have a severely curtailed replicative life span (12). Thrombospondin 1 (TSP1) abundance is inversely correlated with proliferation in some cell types (13). However, insight into TSP1-suppressed proliferation remains unknown.

As reported by Harman (14), oxidative stress has been considered a key driver of the aging process, and subsequent studies have inferred a link between oxidative stress and senescence. Of the highly conserved family of NADPH (reduced form of nicotinamide adenine dinucleotide phosphate) oxidase (Nox) isozymes, which produce reactive oxygen species (ROS), two isoforms are generally considered as promitotic and are pivotal to several pathologies involving hyperproliferation. Accordingly, interest in Nox inhibitor development has intensified and therefore represents an opportunity to interrogate, with therapeutic translation, the link between ROS and aging (15). Here, we present data suggesting a causal role of TSP1-induced increase in the abundance of Nox1 (but not the closely related Nox2, Nox4, or Nox5) in cellular senescence across a wide range of ages in humans, thus challenging the dogma of a primarily pro-proliferative and proapoptotic role for Nox1. We

provide mechanistic insight into senescence triggered by p53-$p21^{cip}$-Rb, and not $p16^{INK4A}$, in human cells and mouse models. We validated our discovery with genetic and pharmacological tools in tissues of humans of increasing age, in mice lacking TSP1 or Nox1, in human endothelial cells challenged with TSP1, and in endothelial cells overexpressing Nox1. Finally, our studies offer an exciting new therapeutic translation of a selective Nox1 inhibitor as a modality to target senescence-associated endothelial dysfunction.

RESULTS

TSP1 is increased in human aging and induces endothelial senescence

Age-related diseases are associated with increased matrix remodeling and matricellular protein abundance (12, 16–19). Of these matricellular proteins, TSP1 is intriguing because of its reported association with age-related pulmonary diseases including pulmonary hypertension, chronic obstructive pulmonary disease, and idiopathic pulmonary fibrosis (20–24). To explore the functional role of TSP1 in aging and disease, we examined whether TSP1 associated with human pulmonary aging by analyzing disease-free lung biopsies (table S1). We observed a strong positive relationship between TSP1 mRNA and increasing age (Fig. 1A), as is suggested by aging muscle data housed at the NCBI (National Center for Biotechnology Information) database (accession #GDS156). Next, we investigated TSP1 localization in pulmonary arteries obtained by rapid autopsy of non–pulmonary-diseased subjects (table S2). Consistently, we observed notable differences in TSP1 immunofluorescence across the vessel wall (Fig. 1B), with a significant increase in intimal TSP1 immunofluorescence in arteries from aged subjects compared to younger controls (Fig. 1C and fig. S1A).

We next explored the functional effects of TSP1 on endothelial cell physiology using primary human pulmonary artery endothelial cells (HPAECs). HPAECs were chosen because they are a well-characterized and readily available model for studying cell-mediated processes in pulmonary disease (25, 26). We found that TSP1 induced cell cycle arrest of HPAECs (Fig. 1D), characterized by increased numbers of cells in G_1-G_0 and decreased numbers of cells in S and G_2-M (Fig. 1E). In line with the ability of TSP1 to block cell proliferation induced by serum, nitric oxide (NO), or fibroblast growth factor 2 (13, 27), TSP1 significantly inhibited HPAEC proliferation, as detected by trypan blue exclusion (Fig. 1F), MTT [3-(4,5-dimethylthiazol-2-yl)-2,5-diphenyltetrazolium bromide] assay (Fig. 1G), and 5-bromo-2′-deoxyuridine (BrdU) incorporation (Fig. 1H). This effect was achieved using a TSP1 concentration (2.2 nM) detected in the plasma of diseased patients (28, 29) and was not enhanced by higher concentrations (fig. S1, B and C).

Blunted proliferation and halted cell cycle progression are hallmarks of cellular senescence (6), a phenotypical switch associated with organismal aging and organ dysfunction (30). To ascertain a functional role for TSP1 in proliferative signaling in vivo and corroborate our primary findings in human cells, we assessed middle-aged (8- to 10-month-old) mouse lungs for proliferating cell nuclear antigen (PCNA) (31) in wild-type and *TSP1*$^{-/-}$ mice (Fig. 2A). Middle-aged mice were chosen because their tissues are terminally differentiated (32), mirroring the early stages of age-related complications in humans (33). Immunoblotting

revealed a significant increase in PCNA abundance in *TSP1*$^{-/-}$ mice compared to age-matched wild-type controls. Accordingly, TSP1 exposure significantly decreased PCNA abundance in HPAECs (Fig. 2B). On the basis of these observations and the increase in expression of self-renewal genes in *CD47*-null endothelial cells (34), we investigated whether TSP1 drove HPAEC senescence. TSP1 exposure significantly increased the number of SA-β-Gal–positive HPAECs and human aortic endothelial cells (Fig. 2C), which showed concentration dependency (fig. S1D), and elicited an enlarged and flattened cell shape characteristic of senescence (Fig. 2D) (35), supporting a work in brain endothelial cells (36). To assess in vivo relevance of our discoveries, we performed SA-β-Gal staining, which was lower in *TSP1*$^{-/-}$ mouse lung tissue than in wild-type mouse lung tissue (Fig. 2E). This observation, coupled with similar collagen staining between the two genotypes (Fig. 2E, blue stain, and fig. S1E), precluded collagen-induced vascular senescence (37). Notably, middle-aged wild-type lungs were abundant in senescent markers, with increased p53 and p21^{cip}, decreased Rb, and no change in p16^{INK4A}, compared to younger controls (fig. S2A). Moreover, aging decreased PCNA abundance in wild-type animals. Because the senescent phenotype is not only associated with cell cycle arrest and cell function decline, we sought to ascertain the role of the senescence-associated secretory phenotype (SASP) components in TSP1-mediated senescence. SASP factors include many inflammatory cytokines, growth factors, and proteases, among others (38–40). Immunoblotting demonstrated that some SASP factors [monocyte chemoattractant protein-1 (MCP-1) and p19^{Arf}] were lower in abundance in *TSP1*$^{-/-}$ lung homogenates compared to those from their wild-type counterparts (Fig. 2F). These observations in aging tissues and endothelial cells support TSP1 as an instigator of cellular senescence.

TSP1 promotes p53-dependent DNA damage response and senescence

The aged pulmonary vascular tree is subject to an imbalance between oxidants and antioxidants and attendant oxidative stress (41), a process associated with the free radical theory of aging (14). Therefore, a link between senescence, oxidative stress, and TSP1 could offer insight into the aging process. In HPAECs exposed to TSP1, $O_2^{\bullet-}$ and H_2O_2 production, both of which are indicators of oxidase activity, were increased (Fig. 2, G and H). Next, we interrogated $O_2^{\bullet-}$ production in middle-aged wild-type and *TSP1*$^{-/-}$ lungs using two complementary assays. *TSP1*$^{-/-}$ lungs displayed significantly lower $O_2^{\bullet-}$ by en face fluorescence (Fig. 2I) and decreased NADPH-driven $O_2^{\bullet-}$ measured by the reduction of cytochrome *c* (Fig. 2J). These findings, together with increased ROS in middle-aged mouse lungs compared to young controls (fig. S2B), suggested a role for TSP1-induced Nox-mediated ROS as a driver of endothelial senescence.

We discovered that TSP1 activated the DNA damage response (DDR) senescence pathway. Rb abundance was reduced, and Ser^{15} in p53 was phosphorylated in HPAECs exposed to TSP1 compared to vehicle control. p53-independent senescence signaling through p16^{INK4A} (18) was excluded because p16^{INK4A} abundance remained unchanged in response to TSP1 (Fig. 3A) and was not increased in middle-aged wild-type mouse lungs (fig. S2A). This finding distinguished TSP1 from other matricellular proteins such as CCN1, which signals through p16^{INK4A} (18). We observed an increase in total p53 and p21^{cip} in middle-aged mice (fig. S2A). Moreover, we discovered that TSP1 exposure increased p53 abundance in

HPAECs in a time-dependent fashion (Fig. 3B) and increased p53 activation, as evidenced by its increased nuclear localization (Fig. 3C). Moreover, TSP1 exposure significantly increased the number of HPAECs positive for $p21^{cip}$ (Fig. 3D), the downstream transcriptional target of p53 activation that encodes a cell cycle–inhibiting factor (42). The increase in the number of SA-β-Gal–positive cells was blocked by p53 silencing, confirming a role for p53 in TSP1-induced endothelial senescence (Fig. 3E and fig. S2C). The abundance of p53 and $p21^{cip}$ was subsequently evaluated in mice. *TSP1*$^{-/-}$ lungs had significantly lower $p21^{cip}$ mRNA (Fig. 3F) and protein (Fig. 3G) abundance compared to age-matched controls, with the abundance of p53 remaining unchanged (Fig. 3, F and G) but active (phosphorylated) p53 decreasing markedly in nulls (Fig. 3G). Because *TSP1*$^{-/-}$ tissue exhibited lower amounts of $O_2^{\bullet-}$ (Fig. 2, I and J), we reasoned that changes in $p21^{cip}$ abundance resulted from a difference in p53 activation, as evidenced by decreased p53-Ser^{15} phosphorylation (Fig. 3G) (43, 44). Because p53 evokes apoptotic signaling, we asked whether TSP1 promoted apoptosis of HPAECs (45). However, apoptosis, as measured by trypan blue cell counting (fig. S3A) and sub–G_1-G_0 FACS quantification (fig. S3B), was unaffected by TSP1 exposure. These observations are consistent with the role of TSP1 in p53-mediated DDR senescence, exclusive of apoptosis.

Aging-linked TSP1-mediated cellular stress is elicited by Nox1

To gain further insight into the mechanisms modulating matricellular-induced cellular $O_2^{\bullet-}$ and DDR-senescence pathway activation, we first sought to identify the receptor responsible for these effects of TSP1. TSP1 reportedly binds and activates several cell-surface receptors, three of which are prominent in the endothelium. A blocking antibody against the cognate TSP1 receptor CD47 attenuated TSP1-induced $O_2^{\bullet-}$ production in HPAECs (Fig. 4A). Moreover, 7N3, a receptor binding peptide that mimics the C-terminal binding domain of TSP1 (46, 47), significantly increased NADPH-dependent $O_2^{\bullet-}$ generation (Fig. 4B). In addition to CD47, the TSP1 receptors signal regulatory protein α (SIRPα) and CD36 are also present in endothelial cells (13, 48, 49). FACS analysis indicated that the abundance of CD47 was similar to that of SIRPα and greater than that of CD36 (fig. S4, A to C). However, antagonizing antibodies against SIRPα and CD36 did not significantly affect $O_2^{\bullet-}$ production (Fig. 4C and fig. S4D). Therefore, of the potential culprits, the TSP1-CD47 axis selectively regulated cellular $O_2^{\bullet-}$ production.

Because TSP1 exposure decreased NO concentrations (fig. S4E), as previously reported (50), we initially postulated that uncoupled endothelial NO synthase (eNOS) could be the major $O_2^{\bullet-}$ source. However, $O_2^{\bullet-}$ concentrations were not affected by the potent eNOS inhibitor N_ω-nitro-L-arginine methyl ester (L-NAME), the mitochondrial inhibitor rotenone, or the xanthine oxidase inhibitor oxypurinol (Fig.4D). In contrast, diphenyleneiodonium (DPI), a broad-profile flavoprotein inhibitor that targets Nox isoforms, ablated TSP1-induced $O_2^{\bullet-}$. We have previously reported that acute TSP1 exposure activates the Nox1 isoform in smooth muscle (46, 49). We thus used our selective Nox1 inhibitor, NoxA1ds (51), and a specific Nox2 inhibitor, Nox2ds-tat (52, 53). TSP1-induced $O_2^{\bullet-}$ production was abolished by the selective Nox1 inhibitor but not by the Nox2-specific inhibitor (Fig. 4E), and the findings with Nox1 were confirmed with siRNA-mediated gene silencing (fig. S4, F

and G). Consequently, these results indicated that Nox1 was the major source of TSP1-induced $O_2^{\bullet-}$ in endothelial cells and potentially a source of aging-induced ROS.

To investigate a link between endothelial senescence and a TSP1-induced increase in Nox-produced ROS, we examined the effects of TSP1 exposure on the abundance of various Nox subunits. Western blot analysis revealed that only the Nox1 catalytic subunit was significantly increased (Fig. 4F). The Nox2 catalytic subunit and NoxO1, the canonical Nox1 organizing subunit, exhibited a tendency toward increased abundance that was not significant, whereas the abundance of the Nox1 activating subunit NoxA1 or the alternate organizer $p47^{phox}$ was unaffected. FACS (Fig. 4G) and mRNA (Fig. 4H) analysis confirmed that TSP1 exposure significantly increased Nox1 abundance. *Nox4* mRNA was significantly increased but to a markedly lower degree and without a corresponding increase in Nox4 protein abundance. Supporting these cellular observations, *Nox1* mRNA abundance was lower in the lungs of middle-aged *TSP1*$^{-/-}$ mice compared to wild-type mice (Fig. 4I). Similarly, we observed that Nox1 protein abundance was significantly lower in middle-aged *TSP1*$^{-/-}$ lungs compared to controls (Fig. 4J), with the abundance of Nox2 and Nox4 remaining unaffected (fig. S4H). In aggregate, these results suggest that Nox1 is the dominant oxidase mediating TSP1-induced endothelial DDR senescence.

Nox1 is a target in human matrix protein–mediated endothelial senescence

We postulated that increased Nox1 abundance was sufficient to induce HPAEC senescence. Nox1 reportedly displays constitutive activity, generating $O_2^{\bullet-}$ because of interactions between the catalytic membrane-spanning Nox1 subunit in association with $p22^{phox}$ and the cytosolic organizing NoxO1 and activator NoxA1 subunits bound through C-terminal interactions with Rac1/2 (54). Consistent with our hypothesis, the number of SA-β-Gal–positive cells was significantly increased in cells transfected with human Nox1 (Fig. 5A) compared to empty plasmid controls. Nox1 overexpression ($Nox1^{OE}$) was confirmed by FACS analysis (fig. S5A) and mirrored increased $O_2^{\bullet-}$ production (Fig. 5B and fig. S5B). Furthermore, middle-aged Nox1-null (*Nox1*$^{-/-}$) mice produced significantly less pulmonary NADPH-driven $O_2^{\bullet-}$ than wild-type mice (Fig. 5C). Moreover, decreased Nox1-derived $O_2^{\bullet-}$ was linked to a significant decrease in $p21^{cip}$ expression without changes in *p53* expression (Fig. 5D). These in vivo results were corroborated with $Nox1^{OE}$ cells, which showed increased $p21^{cip}$ abundance and decreased Rb phosphorylation (fig. S5C). To confirm the role of Nox1 as a potential therapeutic strategy in age-related TSP1-induced senescence, we investigated the ability of the selective Nox1 inhibitor NoxA1ds to attenuate the effects of TSP1 in vitro. In both the MTT-based assay (Fig. 5E) and trypan blue assay (Fig. 5F), NoxA1ds reversed the ability of TSP1 to inhibit endothelial cell proliferation. Moreover, NoxA1ds treatment restored normal cell cycle progression in HPAECs exposed to TSP1 (Fig. 5G). In contrast, $Nox1^{OE}$ reduced cell proliferation (fig. S5D) and cell cycle progression (fig. S5E). Consistent with the notion that TSP1-induced senescence was Nox1-mediated, TSP1 promoted increased p53 nuclear localization and $p21^{cip}$ induction in control cells (Fig. 5H, top), effects that were abrogated by Nox1 inhibition (Fig. 5H, bottom). Moreover, NoxA1ds restored PCNA abundance in TSP1-challenged cells (fig. S5F). These findings support a model in which Nox1 orchestrates TSP1-induced endothelial cell senescence through a DDR-dependent mechanism.

Translational relevance of our in vitro and in vivo findings was further assessed in human lung biopsies from disease-free subjects and mice of varying ages. We detected a strong correlation between the rates of generation of $O_2^{\bullet-}$ (Fig. 6A) and its metabolite H_2O_2 (Fig. 6B) in human lung homogenate with advancing age. We also addressed whether Nox1 abundance was increased with advancing human age because of growing evidence for a role for Nox1 in promoting myriad pathologies (55–59). We showed a significant correlation between increasing age and the abundance of Nox1 protein (Fig. 6C) and a trend toward an increase in mRNA (fig. S6A) in humans. No significant change in protein was observed with other vascular isoforms (Nox2, Nox4, or Nox5; fig. S6, B to E). An increase in Nox1 abundance but not that of Nox2 or Nox4 was also corroborated in middle-aged mouse lungs compared to young controls (fig. S6F). Accordingly, human aging correlated significantly with the abundance of p53 and $p21^{cip}$ (Fig. 6D). Further supporting the potential clinical relevance of our findings, we discovered that Nox1 localized predominantly in the intima of human pulmonary arteries (Fig. 6E, top) and was significantly increased in samples from older subjects compared to those from younger subjects. Similarly, confocal visualization identified increased $p21^{cip}$ with human age in the intimal endothelium (Fig. 6E, bottom), consistent with the clinical translation potential of this pathway. Finally, we confirmed that Nox1 mediated the senescence phenotype in response to TSP1 because NoxA1ds attenuated TSP1-induced senescence in HPAECs (Fig. 6F). Together, these results highlight a role for Nox1 in aging-associated endothelial p53-mediated activation of the DDR pathway and in driving a prosenescent phenotype. Furthermore, agents targeting Nox1 hold promise for slowing or averting this cell fate.

DISCUSSION

Cell senescence is a major hallmark and underpinning of age and premature death. Undoubtedly, over the past two centuries, mankind has seen major improvements in life span, largely as a result of treatment of targeted organ dysfunction and disease. Now, however, there is reasonable concern that extant drug regimens have become so effective that new strategies will yield incremental or, in combination, deleterious effects. Thus, a more fundamental and mechanistic inquiry into the root cause of organismal decline might be expected to yield substantively greater gains in the length and quality of life. With an aging global population, a better understanding of the fundamental mechanisms underlying age-related senescence is of paramount importance (60). We proffer that the study of the actions of matricellular proteins in aging could advance our knowledge of this process. Matricellular proteins increase with age (61), but a causal, rather than a circumstantial, relationship has not been investigated to date.

Associations between increasing age and cardiovascular complications are particularly striking (2, 62, 63). Thus, improved mechanistic insight and identification of molecular targets in age-related vascular disease are critical. Cellular senescence, occurring when cells withdraw from the cell cycle and lose the capacity to proliferate in response to growth factors or mitogens (6), was first described in rapidly replicating human fibroblasts. Senescence is an irreversible form of cell cycle arrest initiated by various stresses, including genotoxic and oxidative stress (9), leading to DNA damage, oncogene activation, and telomere shortening (10). However, endothelial cell senescence may be considered

protective in its ability to stave off vascularization and, in turn, blunt tumor growth (64). On balance, however, augmented senescence with age is deleterious to organ function vis-à-vis interference with tissue self-renewal. Here, we discovered that the matricellular protein TSP1 played a role in human endothelial senescence by increasing the abundance and activation of the Nox1 isozyme. In turn, Nox1-dependent ROS led to p53-$p21^{cip}$-Rb DDR pathway activation and endothelial cell senescence (Fig. 7). This pathway was interrogated using (i) human clinical biopsies and pulmonary artery samples, (ii) genetically modified middle-aged mice lacking TSP1 or Nox1, (iii) primary human endothelial cells, and (iv) human Nox1-overexpressing endothelial cells. Supporting the impact of our findings, translational application was demonstrated using a selective Nox1 inhibitor in human cells.

Findings of increased TSP1 abundance in aged mouse cardiac tissue (65) sparked our interest into the role of TSP1 in the decline of cellular and organ function in the aging process. Here, we discovered a link between age and TSP1 abundance in human lung biopsies, which aligns mechanistically with TSP1-induced human endothelial cell cycle arrest and decreased proliferation corroborated by three independent methods (Fig. 1). These data were supported by a mouse model of aging in vivo, in which deletion of TSP1 resulted in increased PCNA abundance. Moreover, in human endothelial cells, TSP1 decreased PCNA abundance and enhanced senescence, as distinguished by β-Gal staining and cell morphology (Fig. 2). Tissues from *TSP1*$^{-/-}$ mice showed decreased senescence compared to those from age-matched wild-type mice. Together, our current findings identified a role for TSP1 in endothelial senescence, which involves cell cycle progression inhibition, oxidative stress, and p53-mediated DDR signaling.

Organ homeostasis is perturbed upon the accumulation of somatic senescent cells in tissues (5, 6). Hence, senescence is considered an inexorable cell fate in mammals and other organisms (30, 66) and represents a maladaptive response leading to dysfunction and vascular disease. One suggested determinant of in vivo senescence at the molecular level corresponds to the accumulation of oxidative damage triggered by a chronic mild increase in ROS (9). These ROS (for example, $O_2^{\bullet-}$ and its more stable and cell-permeant H_2O_2 product) can impair normal cellular processes by oxidizing macromolecules and damaging organelles (67) and have been associated with disease progression (41). Our data align with the free radical theory of aging in two ways. We discovered a key relationship between age, Nox1, and human lung ROS (Fig. 6). Second, our findings support matricellular TSP1 inducing human endothelial cell ROS and senescence, along with an exhibited suppression of $O_2^{\bullet-}$ production in *TSP1*$^{-/-}$ mouse lungs (Fig. 2). Our findings, combined with reduced senescence and SASP factors in these knockout animals, underscore a functional link between TSP1, Nox1, and senescence.

Of the macromolecules altered by ROS, dysfunctional oxidized DNA repair commits cells to senescence through activation of the DDR pathway, a phenomenon that has been observed in various forms of cancer, neurodegenerative disorders, and infertility (68, 69). A common ancestral feature shared in DDR senescence is the effector p53 (67), which, after Ser^{15} phosphorylation, facilitates S-phase transition blockade through transcriptional regulation of $p21^{cip}$ (44). In cultured HPAECs, we observed a time-dependent increase in p53 abundance and activation (as visualized by nuclear localization) and reversal of TSP1-induced

senescence by p53 knockdown (Fig. 3). We ruled out apoptosis in this response by trypan blue exclusion and FACS (fig. S3). These findings were corroborated in middle-aged mice by demonstrating that *TSP1* deficiency suppressed the abundance of $p21^{cip}$ but not that of p53 (Fig. 3). In human biopsies, we observed a correlation between TSP1 induction of p53-mediated senescence and increasing age (Fig. 6).

Senescence relies on two main molecular pathways: $p16^{INK4A}$-Rb and p53-$p21^{cip}$-Rb signaling. Both pathways converge at the level of Rb, and hypophosphorylated Rb with p53 indicates committed senescence (42). TSP1 promoted p53-$p21^{cip}$-Rb–dependent senescence independently of $p16^{INK4A}$-Rb. These findings contrast with the effects of CCN1, another matricellular protein that promotes both p53- and $p16^{INK4A}$-dependent fibroblast senescence (18), and may suggest a greater role for TSP1 in committed senescence. However, these disparate signaling effects could be cell- and context-dependent and perhaps hinge on the components in a specific milieu of other pro-proliferative and senescence factors. Moreover, given that p53 increases the intracellular abundance of TSP1, which stabilizes p53 tumor suppressor activity (20), it is tempting to speculate that a vicious cycle of TSP1-Nox1-p53 signaling is set in motion. Further studies are warranted to explore this phenomenon.

We have previously reported that TSP1 induces cellular ROS (46, 49). In contrast, the endothelial cell response described here differs in its robust and sustained cumulative signal necessary for senescence induction. We provided evidence to show that TSP1 promoted specific human endothelial Nox1-derived ROS generation through CD47 but not SIRPα receptor engagement. These conclusions are drawn from (i) an observed increase in only Nox1 in HPAECs by Western blot, FACS, and mRNA analysis; (ii) effective inhibition and induction of ROS by blocking and stimulating CD47, respectively; and (iii) the ability of the Nox1-specific inhibitor NoxA1ds, but not of Nox2ds-tat (which is Nox2-specific), to suppress ROS (Fig. 4). The latter was corroborated using Nox1 siRNA (fig. S4). Moreover, TSP1 knockdown in aged mice elicited a decrease in Nox1 (but not in Nox2 or Nox4) at the mRNA and protein levels. Endothelial Nox1 (58, 70) exists in a constitutively active form or an inducible form (71). Because we discovered that human and murine aging, as well as TSP1 exposure, increased Nox1 abundance, we assert that the increase in ROS we observed is attributable to constitutive and chronic Nox1 activity. Thus, we submit that this chronic ROS generation, in turn, persistently drives DDR-related endothelial senescence (59).

Our findings that human Nox1 overexpression ($Nox1^{OE}$) in HPAECs augmented the senescent phenotype are consistent with our observations of increased Nox1 abundance in aged human lung vasculature and after TSP1 challenge. Moreover, $Nox1^{-/-}$ deficiency lowered ROS production and $p21^{cip}$ abundance in middle-aged mice. In human cells, Nox1 inhibition reversed the ability of TSP1 to suppress proliferation and cell cycle progression and induce p53 nuclear localization and $p21^{cip}$-positive cells. Further, overexpressing Nox1 resulted in increased ROS production, senescence, $p21^{cip}$ abundance, and Rb hypophosphorylation, consistent with a role of Nox1 in these processes (Fig. 5 and fig. S5). Together, these findings support the role of Nox1 in propagating endothelial ROS-induced senescence.

Finally, clinical and therapeutic implications of our findings were illustrated by age-dependent increases in two readouts of Nox-derived ROS production ($O_2^{\bullet -}$ and H_2O_2) in human lungs, along with robust increases in Nox1, p53, and $p21^{cip}$ (Fig. 6). Complementing these data further were cross sections of pulmonary artery illustrating a higher abundance of Nox1 and $p21^{cip}$ in the luminal endothelium. Finally, targeting Nox1 with its specific inhibitor NoxA1ds quelled senescence of human endothelial cells.

Members of the Nox family of isozymes, namely, Nox1, Nox2, and Nox4, have roles in proliferation and vessel remodeling (33, 72, 73). Thus, we did not expect Nox enzymes to play a role in aging-associated senescence. Finally, the specific transcriptional activators that increase Nox1 expression in the aging process will require exploration. The Nox1 promoter is reportedly responsive to various factors (74).

In summary, we found that a matricellular protein–induced, Nox1-derived ROS was responsible for p53-$p21^{cip}$-Rb signaling and senescence, which were attenuated by Nox1 inhibition. Our findings linking TSP1/CD47, Nox1, and p53/p21/Rb to senescence in animal and human cells and during aging in human tissues are unique and previously unreported from both a mechanistic and a clinical standpoint. Finally, the exogenous delivery of Nox1 inhibitor(s) could offer therapeutic utility in the aging lung and other age-related pathologies.

MATERIALS AND METHODS

Materials and reagents

Cytochrome *c*, superoxide dismutase (SOD), catalase, DPI, L-NAME, rotenone, phenylmethylsulfonyl fluoride (PMSF), β-Gal, and other reagents were purchased from Sigma-Aldrich. Amplex Red and propidium iodide were purchased from Invitrogen. Protease and phosphatase inhibitor cocktail tablets were purchased from Roche Diagnostics GmbH. Human TSP1 was purchased from Athens Research and Technology. Peptide 7N3 (RFYVVMYEGKK) was synthesized by Peptides International Inc. BrdU cell proliferation kit was from Cell Signaling Technology.

Human samples

The study was approved by the University of Pittsburgh Institutional Review Board, and written informed consent was obtained from all participating individuals. Lung and pulmonary artery (fifth branch) tissues from control non–pulmonary-diseased lung donors were provided by the PACCM (Division of Pulmonary, Allergy and Critical Care Medicine) Bio-Bank under protocols approved by the University of Pittsburgh Institutional Review Board. Tissues were harvested in optimal cutting temperature (OCT) medium, frozen, and sectioned (8 μm) for subsequent analysis (see below).

Animals

All animal studies were performed under a protocol approved by the Institutional Animal Care and Use Committee of the University of Pittsburgh. *TSP1*$^{-/-}$ and *Nox1*$^{-/-}$ mice (8 to 10 months old) on a C57BL/6 background, and age-matched wild-type C57BL/6 control mice

were purchased from the Jackson Laboratory. Animals were sacrificed, and lungs were collected and either snap-frozen or embedded in OCT medium and frozen for further analysis.

HPAEC culture, TSP1 challenge, blocking antibody experiments, and NoxA1ds treatment

HPAECs (Lonza) were grown in EBM-2 (endothelial growth basal medium-2) containing EGM-2 (endothelial cell growth medium-2) BulletKit components (Lonza). Cells (passages 3 to 6) were seeded the day before the experimentation and synchronized in serum-reduced medium (1% fetal bovine serum) for 4 hours. Synchronized endothelial cells were treated with vehicle or TSP1 (2.2 nM) for 24 hours (or as indicated) and subjected to either homogenization in ice-cold disruption buffer (Hanks' balanced salt solution containing 1.8 mM $CaCl_2$, 0.8 mM $MgCl_2$, and 0.1 mM PMSF), fixation in 2% paraformaldehyde/phosphate-buffered saline (PBS), or trypsinized for intact cell analysis. In some studies, blocking antibodies to CD47 (clone B6H12, Santa Cruz Biotechnology), SIRPα (clone C20, Santa Cruz Biotechnology), or CD36 (clone H-300, Santa Cruz Biotechnology) were added to the cell culture medium (1 mg/ml) for 3 min before TSP1 challenge. In addition, specific inhibition of the Nox1 enzyme was achieved using the NoxA1ds (10 μM) peptide (51) or its scrambled-ds peptide control (10 μM). In these experiments, cells were pretreated with peptides for 1 hour before TSP1 (2.2 nM) challenge.

siRNA gene silencing and Nox1 plasmid transfection

HPAECs were seeded at a density to achieve a 75 to 80% confluence overnight and were subjected to either p53 or Nox1 siRNA transfection (Santa Cruz Biotechnology) using the Lipofectamine 2000 transfection reagent (Invitrogen) according to the manufacturer's protocol, as documented previously (51). To control for possible nonspecific effects of siRNA, control siRNA was used. Gene silencing was confirmed using immunoblotting, and the knockdown was expressed as a fold of siRNA controls. $Nox1^{OE}$ was achieved by transfecting cells with human Nox1 or an empty plasmid vector control, as published previously (75).

Cell proliferation assay

The in vitro proliferative capacity of HPAECs was analyzed using three independent assays. MTT proliferation assay was performed as described previously. Briefly, HPAECs were suspended in EGM-2–containing EBM-2 and plated on flat-bottomed 96-well plates at a density of 1×10^5 cells per well in triplicate. After overnight seeding (16 hours), cells were challenged with TSP1 (2.2 nM), and proliferation was assessed using MTT (Sigma-Aldrich) assay. Absorbance at 570 nm was read using a plate reader (BioTek Synergy 4 Hybrid Multi-Mode Microplate Reader), and the proliferation index was calculated relative to the absorbance value of the vehicle-treated controls. Trypan blue exclusion assay was performed as documented previously (76). Briefly, TSP1 (2.2 nM) was added to cultures of HPAECs for indicated periods after an overnight seeding and a 4-hour synchronization. Subsequently, cells were trypsinized, 10 μl of trypan blue (4% solution) was added to an equal volume of cell suspension, and cell numbers were counted using a hemocytometer. Cell numbers were normalized and expressed as a fold change over time from the start of the experiment (time, 0 hour). BrdU assay was performed as per the manufacturer's instructions.

Cell cycle analysis

HPAECs were treated with TSP1 (2.2 nM; 24 hours), trypsinized, and analyzed for cell cycle phase analysis, as described previously (76). Briefly, after fixation in ice-cold 70% ethanol/PBS, cells were treated with ribonuclease A (0.2 mg/ml), and DNA content was stained with propidium iodide (50 μg/ml) at room temperature for 45 min. The number of cells in G_0-G_1, S, and G_2-M phases and sub–G_0-G_1 apoptotic cells (77) was counted using a BD LSRFortessa flow cytometer and analyzed using the FlowJo software (version 10). A minimum of 10,000 events was recorded for each sample and are expressed as a percentage for each cell cycle phase.

Immunofluorescence

Immunofluorescence microscopy was performed as described previously using endothelial cells cultured on 1% gelatin–coated chamber slides (78, 79). Primary antibodies were used at a 1:200 dilution in PBS with 0.1% bovine serum albumin (BSA) for 60 min at room temperature after a 15-min permeabilization of the cells in 0.25% Triton X-100 and 0.5% BSA/PBS. Species-specific fluorochrome-conjugated secondary antibodies (1:500) were applied to detect specific antigen localization, using fluorescein isothiocyanate (FITC) (green), Cy3 (red), and Cy5 (gray) as fluorochromes. DAPI (blue) was used to visualize the nuclei. Normal rabbit or goat immunoglobulin G (5 μg/ml) was used in the place of primary antibody as a negative control. Images were acquired on an Olympus FluoView-II inverted confocal microscope system and stored digitally for analysis. For immunofluorescence labeling of lung and pulmonary artery sections, 5-μm sections of OCT-embedded tissue were first washed with PBS and blocked in 10% BSA/PBS solution for 30 min at room temperature after permeabilization. To detect specific antigens, the staining procedure was performed as described above.

SA-β-Gal staining

HPAEC and lung senescence analysis was performed as detailed previously (35, 80). Briefly, samples were fixed in a 2% paraformaldehyde/PBS (pH 7.4) solution for 15 min at room temperature, washed in PBS twice, and then incubated with the freshly prepared SA-β-Gal staining solution [citric acid/sodium phosphate buffer (pH 6.0) containing X-Gal (1 mg/ml), 5 mM $Fe(CN)_6^{3-}$, 5 mM $Fe(CN)_6^{4-}$, 150 mM NaCl, and 2 mM $MgCl_2$] for 24 hours in a humidified chamber placed in a non-CO_2 incubator to maintain a buffered solution at pH 6.0. The following day, samples were washed in PBS twice, and images were captured at random using a light microscope (Leica Imaging Systems Ltd.). At least six images representing each condition were captured from each well and were blindly assessed for SA-β-Gal (blue)–positive cells.

Immunoblotting

Total cell and lung homogenates were generated as described previously (78). Soluble protein concentrations of the homogenates were determined using a plate-based Bradford assay kit (Thermo Fisher Scientific). Immunoblotting was conducted by loading 35 μg of protein per lane, as described previously (46). The images were captured digitally using a LI-COR biotechnology system, and the optical density of the protein bands was normalized

to the loading control bands (quantified using ImageJ). Results were normalized to β-actin loading controls in each gel and expressed as a fold change from vehicle treatment.

FACS analysis of receptor and protein expression

CD47, SIRPα, and CD36 were assessed by FACS, as published previously (81). Briefly, intact HPAECs after trypsinization were incubated with primary antibodies, washed, and incubated with fluorescently labeled secondary antibodies with either FITC or Cy5. In some cases, notably when detecting Nox1, $p21^{cip}$, or phospho-Rb by FACS, cellular permeabilization in 0.25% Triton X-100/PBS and blocking in 1% BSA/PBS for 30 min on ice were required. After antibody labeling, cells were counted using a BD LSRFortessa flow cytometer and analyzed using the FlowJo software (version 10). A minimum of 10,000 events were recorded for each sample.

ROS measurement

ROS production in endothelial cells was measured using four independent complementary assays. $O_2^{\bullet-}$ production by total cellular homogenates was measured by cytochrome *c* reduction, as described previously (46). $O_2^{\bullet-}$ production was initiated by the addition of 180 μM NADPH and was calculated from the initial linear rate of SOD (150 U/ml)–inhibitable cytochrome *c* reduction quantified at 550 nm and using an extinction coefficient of 21.1 mM^{-1} cm^{-1} (BioTek Synergy 4 Hybrid Multi-Mode Microplate Reader). Potential enzymatic sources of $O_2^{\bullet-}$ production were also investigated by using the following inhibitors: DPI (20 μM; flavoproteins), L-NAME (100 μM; NO synthases), rotenone (50 μM; mitochondrial complex I), or oxypurinol (100 μM; xanthine oxidase). Endothelial cell homogenate H_2O_2 production was measured using the Amplex Red (Invitrogen Inc.) assay, as described previously. Briefly, protein (50 μg/ml) was added to the wells on a 96-well plate containing the assay mixture [25 mM Hepes (pH 7.4) containing 0.12 M NaCl, 3 mM KCl, 1 mM $MgCl_2$, 0.1 mM Amplex Red, and horseradish peroxidase (0.32 U/ml)]. The reaction was initiated by the addition of 36 μM NADPH, as published previously (46). Fluorescence was detected using the BioTek Synergy 4 Hybrid Multi-Mode Microplate Reader with a 530/25 excitation and a 590/35 emission filter. The reaction was monitored for 30 min at 25°C; the change in emission intensity was linear during this interval. To confirm the H_2O_2 signal, catalase (300 U/ml) was added in parallel wells, and the catalase-inhibitable rate of H_2O_2 production was quantified from an H_2O_2 standard curve. Lung ROS generation was investigated using the cytochrome *c* assay in total lung homogenates (see above), as well as using in situ DHE analysis of OCT-embedded mouse lung sections. Briefly, 5-μm-thick lung sections were incubated at room temperature with DHE (10 μM) for 30 min. Sections were examined by fluorescence microscopy (Leica Imaging Systems Ltd.), and fluorescence (490/580-nm excitation/emission wavelengths) intensity from 20 fields of lung sections was evaluated using the ImageJ software. In parallel sections, Tiron (cell-permeant $O_2^{\bullet-}$ scavenger; 10 mM) was added to determine the proportion of DHE fluorescence that was $O_2^{\bullet-}$-dependent. Results obtained from fluorescence imaging are expressed as Tiron-inhibitable fluorescence intensity. Finally, to corroborate the results, ROS production was assessed by lucigenin-enhanced luminescence assay, as published previously (81).

Quantitative reverse transcription polymerase chain reaction

Total RNA was extracted from lung tissues using the RNeasy Plus kit (Qiagen) as per the manufacturer's protocol. Total RNA was reverse-transcribed to complementary DNA by using SuperScript III (Invitrogen Inc.) following the manufacturer's protocol. For qRT-PCR, commercially available primers for *TSP1*, *Nox1*, *p53*, and $p21^{cip}$ (Invitrogen Inc.) were used. All results were normalized to the housekeeping gene *18S*, and relative quantification was obtained using the ΔC_t (threshold cycle) method; relative expression was calculated as $2^{-\Delta\Delta Ct}$.

Statistics

Data are means ± SEM of the results from at least three independent cell cultures, at least four to six animals per group, or six to eight human samples per group, as detailed in the figure legends. Comparisons were made by unpaired Student's *t* test, Mann-Whitney test, linear regression, repeated-measures analysis, or one-way ANOVA. $P < 0.05$ was considered statistically significant.

Supplementary Material

Refer to Web version on PubMed Central for supplementary material.

Acknowledgments

We thank R. A. Bilonick for the constructive comments and C. Monzo for the assistance with the editing of this manuscript.

Funding: This work was supported by NIH grants R01HL112914, R01HL079207, P01HL103455, and T32 GM008424 (to P.J.P.); AHA-15SDG24910003 (to I.A.G.); R01HL108954, 1R01HL112914-01A1, and 1R21EB017184-01A1 (to J.S.I.); R42-AA024003 and R01-CA162306 (to M.M.R.); 2R01HL098032, 1R01HL125886-01, P01HL103455, T32 HL110849, and T32 HL007563 (to M.T.G.); and 5 K23 HL112848-03 6 (to E.M.N.). This study was supported by the Institute for Transfusion Medicine and the Hemophilia Center of Western Pennsylvania.

REFERENCES AND NOTES

1. Christensen K, Doblhammer G, Rau R, Vaupel JW. Ageing populations: The challenges ahead. Lancet. 2009; 374:1196–1208. [PubMed: 19801098]
2. Tuder RM, Petrache I. Pathogenesis of chronic obstructive pulmonary disease. J Clin Invest. 2012; 122:2749–2755. [PubMed: 22850885]
3. Gellie A, Mills A, Levinson M, Stephenson G, Flynn E. Death: A foe to be conquered? Questioning the paradigm. Age Ageing. 2015; 44:7–10. [PubMed: 25225350]
4. Benetos A, Rossignol P, Cherubini A, Joly L, Grodzicki T, Rajkumar C, Strandberg TE, Petrovic M. Polypharmacy in the aging patient: Management of hypertension in octogenarians. JAMA. 2015; 314:170–180. [PubMed: 26172896]
5. Childs BG, Durik M, Baker DJ, van Deursen JM. Cellular senescence in aging and age-related disease: From mechanisms to therapy. Nat Med. 2015; 21:1424–1435. [PubMed: 26646499]
6. Muñoz-Espín D, Serrano M. Cellular senescence: From physiology to pathology. Nat Rev Mol Cell Biol. 2014; 15:482–496. [PubMed: 24954210]
7. Boe AE, Eren M, Murphy SB, Kamide CE, Ichimura A, Terry D, McAnally D, Smith LH, Miyata T, Vaughan DE. Plasminogen activator inhibitor-1 antagonist TM5441 attenuates N^{ω}-nitro-L-arginine methyl ester–induced hypertension and vascular senescence. Circulation. 2013; 128:2318–2324. [PubMed: 24092817]

8. Wang J, Uryga AK, Reinhold J, Figg N, Baker L, Finigan A, Gray K, Kumar S, Clarke M, Bennett M. Vascular smooth muscle cell senescence promotes atherosclerosis and features of plaque vulnerability. Circulation. 2015; 132:1909–1919. [PubMed: 26416809]

9. Kurz DJ, Decary S, Hong Y, Trivier E, Akhmedov A, Erusalimsky JD. Chronic oxidative stress compromises telomere integrity and accelerates the onset of senescence in human endothelial cells. J Cell Sci. 2004; 117:2417–2426. [PubMed: 15126641]

10. Fyhrquist F, Saijonmaa O, Strandberg T. The roles of senescence and telomere shortening in cardiovascular disease. Nat Rev Cardiol. 2013; 10:274–283. [PubMed: 23478256]

11. Acosta JC, Banito A, Wuestefeld T, Georgilis A, Janich P, Morton JP, Athineos D, Kang TW, Lasitschka F, Andrulis M, Pascual G, Morris KJ, Khan S, Jin H, Dharmalingam G, Snijders AP, Carroll T, Capper D, Pritchard C, Inman GJ, Longerich T, Sansom OJ, Benitah SA, Zender L, Gil J. A complex secretory program orchestrated by the inflammasome controls paracrine senescence. Nat Cell Biol. 2013; 15:978–990. [PubMed: 23770676]

12. Murano S, Thweatt R, Shmookler Reis RJ, Jones RA, Moerman EJ, Goldstein S. Diverse gene sequences are overexpressed in werner syndrome fibroblasts undergoing premature replicative senescence. Mol Cell Biol. 1991; 11:3905–3914. [PubMed: 1712899]

13. Isenberg JS, Ridnour LA, Perruccio EM, Espey MG, Wink DA, Roberts DD. Thrombospondin-1 inhibits endothelial cell responses to nitric oxide in a cGMP-dependent manner. Proc Natl Acad Sci USA. 2005; 102:13141–13146. [PubMed: 16150726]

14. Harman D. The aging process. Proc Natl Acad Sci USA. 1981; 78:7124–7128. [PubMed: 6947277]

15. Cifuentes-Pagano E, Meijles DN, Pagano PJ. The quest for selective nox inhibitors and therapeutics: Challenges, triumphs and pitfalls. Antioxid Redox Signal. 2014; 20:2741–2754. [PubMed: 24070014]

16. Boon RA, Iekushi K, Lechner S, Seeger T, Fischer A, Heydt S, Kaluza D, Tréguer K, Carmona G, Bonauer A, Horrevoets AJG, Didier N, Girmatsion Z, Biliczki P, Ehrlich JR, Katus HA, Müller OJ, Potente M, Zeiher AM, Hermeking H, Dimmeler S. MicroRNA-34a regulates cardiac ageing and function. Nature. 2013; 495:107–110. [PubMed: 23426265]

17. Dai DF, Santana LF, Vermulst M, Tomazela DM, Emond MJ, MacCoss MJ, Gollahon K, Martin GM, Loeb LA, Ladiges WC, Rabinovitch PS. Overexpression of catalase targeted to mitochondria attenuates murine cardiac aging. Circulation. 2009; 119:2789–2797. [PubMed: 19451351]

18. Jun JI, Lau LF. The matricellular protein CCN1 induces fibroblast senescence and restricts fibrosis in cutaneous wound healing. Nat Cell Biol. 2010; 12:676–685. [PubMed: 20526329]

19. Rogers NM, Roberts DD, Isenberg JS. Age-associated induction of cell membrane CD47 limits basal and temperature-induced changes in cutaneous blood flow. Ann Surg. 2013; 258:184–191. [PubMed: 23275312]

20. Baek KH, Bhang D, Zaslavsky A, Wang LC, Vachani A, Kim CF, Albelda SM, Evan GI, Ryeom S. Thrombospondin-1 mediates oncogenic *Ras*-induced senescence in premalignant lung tumors. J Clin Invest. 2013; 123:4375–4389. [PubMed: 24018559]

21. Bauer PM, Bauer EM, Rogers NM, Yao M, Feijoo-Cuaresma M, Pilewski JM, Champion HC, Zuckerbraun BS, Calzada MJ, Isenberg JS. Activated CD47 promotes pulmonary arterial hypertension through targeting caveolin-1. Cardiovasc Res. 2012; 93:682–693. [PubMed: 22215724]

22. Lee JH, Bhang DH, Beede A, Huang TL, Stripp BR, Bloch KD, Wagers AJ, Tseng YH, Ryeom S, Kim CF. Lung stem cell differentiation in mice directed by endothelial cells via a BMP4-NFATc1-thrombospondin-1 axis. Cell. 2014; 156:440–455. [PubMed: 24485453]

23. Rogers NM, Yao M, Sembrat J, George MP, Knupp H, Ross M, Sharifi-Sanjani M, Milosevic J, St Croix C, Rajkumar R, Frid MG, Hunter KS, Mazzaro L, Novelli EM, Stenmark KR, Gladwin MT, Ahmad F, Champion HC, Isenberg JS. Cellular, pharmacological, and biophysical evaluation of explanted lungs from a patient with sickle cell disease and severe pulmonary arterial hypertension. Pulm Circ. 2013; 3:936–951. [PubMed: 25006410]

24. Wang IM, Stepaniants S, Boie Y, Mortimer JR, Kennedy B, Elliott M, Hayashi S, Loy L, Coulter S, Cervino S, Harris J, Thornton M, Raubertas R, Roberts C, Hogg JC, Crackower M, O'Neill G, Paré PD. Gene expression profiling in patients with chronic obstructive pulmonary disease and lung cancer. Am J Respir Crit Care Med. 2008; 177:402–411. [PubMed: 17975202]

25. Lathen C, Zhang Y, Chow J, Singh M, Lin G, Nigam V, Ashraf YA, Yuan JX, Robbins IM, Thistlethwaite PA. ERG-APLNR axis controls pulmonary venule endothelial proliferation in pulmonary veno-occlusive disease. Circulation. 2014; 130:1179–1191. [PubMed: 25062690]
26. Xu W, Koeck T, Lara AR, Neumann D, DiFilippo FP, Koo M, Janocha AJ, Masri FA, Arroliga AC, Jennings C, Dweik RA, Tuder RM, Stuehr DJ, Erzurum SC. Alterations of cellular bioenergetics in pulmonary artery endothelial cells. Proc Natl Acad Sci USA. 2007; 104:1342–1347. [PubMed: 17227868]
27. Iruela-Arispe ML, Lombardo M, Krutzsch HC, Lawler J, Roberts DD. Inhibition of angiogenesis by thrombospondin-1 is mediated by 2 independent regions within the type 1 repeats. Circulation. 1999; 100:1423–1431. [PubMed: 10500044]
28. Brostjan C, Bayer A, Zommer A, Gornikiewicz A, Roka S, Benkö T, Yaghubian R, Jakesz R, Steger G, Gnant M, Friedl J, Stift A. Monitoring of circulating angiogenic factors in dendritic cell–based cancer immunotherapy. Cancer. 2003; 98:2291–2301. [PubMed: 14601101]
29. Novelli EM, Kato GJ, Ragni MV, Zhang Y, Hildesheim ME, Nouraie M, Barge S, Meyer MP, Hassett AC, Gordeuk VR, Gladwin MT, Isenberg JS. Plasma thrombospondin-1 is increased during acute sickle cell vaso-occlusive events and associated with acute chest syndrome, hydroxyurea therapy, and lower hemolytic rates. Am J Hematol. 2012; 87:326–330. [PubMed: 22318901]
30. van Deursen JM. The role of senescent cells in ageing. Nature. 2014; 509:439–446. [PubMed: 24848057]
31. Waga S, Hannon GJ, Beach D, Stillman B. The p21 inhibitor of cyclin-dependent kinases controls DNA replication by interaction with PCNA. Nature. 1994; 369:574–578. [PubMed: 7911228]
32. Warburton D, El-Hashash A, Carraro G, Tiozzo C, Sala F, Rogers O, De Langhe S, Kemp PJ, Riccardi D, Torday J, Bellusci S, Shi W, Lubkin SR, Jesudason E. Lung organogenesis. Curr Top Dev Biol. 2010; 90:73–158. [PubMed: 20691848]
33. Tickner J, Fan LM, Du J, Meijles D, Li JM. Nox2-derived ROS in PPARγ signaling and cell-cycle progression of lung alveolar epithelial cells. Free Radic Biol Med. 2011; 51:763–772. [PubMed: 21664456]
34. Kaur S, Soto-Pantoja DR, Stein EV, Liu C, Elkahloun AG, Pendrak ML, Nicolae A, Singh SP, Nie Z, Levens D, Isenberg JS, Roberts DD. Thrombospondin-1 signaling through CD47 inhibits self-renewal by regulating c-Myc and other stem cell transcription factors. Sci Rep. 2013; 3:1673. [PubMed: 23591719]
35. Dimri GP, Lee X, Basile G, Acosta M, Scott G, Roskelley C, Medrano EE, Linskens M, Rubelj I, Pereira-Smith O, Peacocke M, Campisi J. A biomarker that identifies senescent human cells in culture and in aging skin in vivo. Proc Natl Acad Sci USA. 1995; 92:9363–9367. [PubMed: 7568133]
36. Gao Q, Chen K, Gao L, Zheng Y, Yang YG. Thrombospondin-1 signaling through CD47 inhibits cell cycle progression and induces senescence in endothelial cells. Cell Death Dis. 2016; 7:e2368. [PubMed: 27607583]
37. Vafaie F, Yin H, O'Neil C, Nong Z, Watson A, Arpino J-M, Chu MWA, Wayne Holdsworth D, Gros R, Pickering JG. Collagenase-resistant collagen promotes mouse aging and vascular cell senescence. Aging Cell. 2014; 13:121–130. [PubMed: 23957394]
38. Coppé JP, Patil CK, Rodier F, Krtolica A, Beauséjour CM, Parrinello S, Hodgson JG, Chin K, Desprez PY, Campisi J. A human-like senescence-associated secretory phenotype is conserved in mouse cells dependent on physiological oxygen. PLOS ONE. 2010; 5:e9188. [PubMed: 20169192]
39. Freund A, Orjalo AV, Desprez PY, Campisi J. Inflammatory networks during cellular senescence: Causes and consequences. Trends Mol Med. 2010; 16:238–246. [PubMed: 20444648]
40. Tchkonia T, Zhu Y, van Deursen J, Campisi J, Kirkland JL. Cellular senescence and the senescent secretory phenotype: Therapeutic opportunities. J Clin Invest. 2013; 123:966–972. [PubMed: 23454759]
41. Holmström KM, Finkel T. Cellular mechanisms and physiological consequences of redox-dependent signalling. Nat Rev Mol Cell Biol. 2014; 15:411–421. [PubMed: 24854789]

42. Leontieva OV, Gudkov AV, Blagosklonny MV. Weak p53 permits senescence during cell cycle arrest. Cell Cycle. 2010; 9:4323–4327. [PubMed: 21051933]
43. Hainaut P, Mann K. Zinc binding and redox control of p53 structure and function. Antioxid Redox Signal. 2001; 3:611–623. [PubMed: 11554448]
44. Ueno M, Masutani H, Arai RJ, Yamauchi A, Hirota K, Sakai T, Inamoto T, Yamaoka Y, Yodoi J, Nikaido T. Thioredoxin-dependent redox regulation of p53-mediated p21 activation. J Biol Chem. 1999; 274:35809–35815. [PubMed: 10585464]
45. Jiménez B, Volpert OV, Crawford SE, Febbraio M, Silverstein RL, Bouck N. Signals leading to apoptosis-dependent inhibition of neovascularization by thrombospondin-1. Nat Med. 2000; 6:41–48. [PubMed: 10613822]
46. Csányi G, Yao M, Rodríguez AI, Al Ghouleh I, Sharifi-Sanjani M, Frazziano G, Huang X, Kelley EE, Isenberg JS, Pagano PJ. Thrombospondin-1 regulates blood flow via CD47 receptor–mediated activation of NADPH oxidase 1. Arterioscler Thromb Vasc Biol. 2012; 32:2966–2973. [PubMed: 23087362]
47. Gao AG, Lindberg FP, Finn MB, Blystone SD, Brown EJ, Frazier WA. Integrin-associated protein is a receptor for the C-terminal domain of thrombospondin. J Biol Chem. 1996; 271:21–24. [PubMed: 8550562]
48. O'Connell BJ, Denis M, Genest J. Cellular physiology of cholesterol efflux in vascular endothelial cells. Circulation. 2004; 110:2881–2888. [PubMed: 15492319]
49. Yao M, Rogers NM, Csányi G, Rodriguez AI, Ross MA, St Croix C, Knupp H, Novelli EM, Thomson AW, Pagano PJ, Isenberg JS. Thrombospondin-1 activation of signal-regulatory protein-α stimulates reactive oxygen species production and promotes renal ischemia reperfusion injury. J Am Soc Nephrol. 2014; 25:1171–1186. [PubMed: 24511121]
50. Isenberg JS, Martin-Manso G, Maxhimer JB, Roberts DD. Regulation of nitric oxide signalling by thrombospondin 1: Implications for anti-angiogenic therapies. Nat Rev Cancer. 2009; 9:182–194. [PubMed: 19194382]
51. Ranayhossaini DJ, Rodriguez AI, Sahoo S, Chen BB, Mallampalli RK, Kelley EE, Csanyi G, Gladwin MT, Romero G, Pagano PJ. Selective recapitulation of conserved and nonconserved regions of putative NOXA1 protein activation domain confers isoform-specific inhibition of Nox1 oxidase and attenuation of endothelial cell migration. J Biol Chem. 2013; 288:36437–36450. [PubMed: 24187133]
52. Csányi G, Cifuentes-Pagano E, Al Ghouleh I, Ranayhossaini DJ, Egaña L, Lopes LR, Jackson HM, Kelley EE, Pagano PJ. Nox2 B-loop peptide, Nox2ds, specifically inhibits the NADPH oxidase Nox2. Free Radic Biol Med. 2011; 51:1116–1125. [PubMed: 21586323]
53. Rey FE, Cifuentes ME, Kiarash A, Quinn MT, Pagano PJ. Novel competitive inhibitor of NAD(P)H oxidase assembly attenuates vascular O_2^- and systolic blood pressure in mice. Circ Res. 2001; 89:408–414. [PubMed: 11532901]
54. Lambeth JD, Neish AS. Nox enzymes and new thinking on reactive oxygen: A double-edged sword revisited. Annu Rev Pathol. 2014; 9:119–145. [PubMed: 24050626]
55. Arnold RS, Shi J, Murad E, Whalen AM, Sun CQ, Polavarapu R, Parthasarathy S, Petros JA, Lambeth JD. Hydrogen peroxide mediates the cell growth and transformation caused by the mitogenic oxidase Nox1. Proc Natl Acad Sci USA. 2001; 98:5550–5555. [PubMed: 11331784]
56. Gray SP, Di Marco E, Okabe J, Szyndralewiez C, Heitz F, Montezano AC, de Haan JB, Koulis C, El-Osta A, Andrews KL, Chin-Dusting JPF, Touyz RM, Wingler K, Cooper ME, Schmidt HHW, Jandeleit-Dahm KA. NADPH oxidase 1 plays a key role in diabetes mellitus–accelerated atherosclerosis. Circulation. 2013; 127:1888–1902. [PubMed: 23564668]
57. Terada LS, Nwariaku FE. Escaping anoikis through ROS: ANGPTL4 controls integrin signaling through Nox1. Cancer Cell. 2011; 19:297–299. [PubMed: 21397852]
58. Wind S, Beuerlein K, Armitage ME, Taye A, Kumar AHS, Janowitz D, Neff C, Shah AM, Wingler K, Schmidt HHW. Oxidative stress and endothelial dysfunction in aortas of aged spontaneously hypertensive rats by NOX1/2 is reversed by NADPH oxidase inhibition. Hypertension. 2010; 56:490–497. [PubMed: 20606112]
59. Zhu K, Kakehi T, Matsumoto M, Iwata K, Ibi M, Ohshima Y, Zhang J, Liu J, Wen X, Taye A, Fan C, Katsuyama M, Sharma K, Yabe-Nishimura C. NADPH oxidase NOX1 is involved in activation

of protein kinase C and premature senescence in early stage diabetic kidney. Free Radic Biol Med. 2015; 83:21–30. [PubMed: 25701431]

60. Kennedy B. Gerontology: More funding for studies of ageing. Nature. 2012; 487:39.
61. Sprenger CC, Plymate SR, Reed MJ. Aging-related alterations in the extracellular matrix modulate the microenvironment and influence tumor progression. Int J Cancer. 2010; 127:2739–2748. [PubMed: 21351253]
62. Qiu C, Fratiglioni L. A major role for cardiovascular burden in age-related cognitive decline. Nat Rev Cardiol. 2015; 12:267–277. [PubMed: 25583619]
63. Sun Z. Aging, arterial stiffness, and hypertension. Hypertension. 2015; 65:252–256. [PubMed: 25368028]
64. Kuilman T, Peeper DS. Senescence-messaging secretome: SMS-ing cellular stress. Nat Rev Cancer. 2009; 9:81–94. [PubMed: 19132009]
65. van Almen GC, Verhesen W, van Leeuwen REW, van de Vrie M, Eurlings C, Schellings MWM, Swinnen M, Cleutjens JPM, van Zandvoort MAMJ, Heymans S, Schroen B. MicroRNA-18 and microRNA-19 regulate CTGF and TSP-1 expression in age-related heart failure. Aging Cell. 2011; 10:769–779. [PubMed: 21501375]
66. Vigneron A, Vousden KH. p53, ROS and senescence in the control of aging. Aging. 2010; 2:471–474. [PubMed: 20729567]
67. Rai P, Onder TT, Young JJ, McFaline JL, Pang B, Dedon PC, Weinberg RA. Continuous elimination of oxidized nucleotides is necessary to prevent rapid onset of cellular senescence. Proc Natl Acad Sci USA. 2009; 106:169–174. [PubMed: 19118192]
68. Borrás C, Gómez-Cabrera MC, Viña J. The dual role of p53: DNA protection and antioxidant. Free Radic Res. 2011; 45:643–652. [PubMed: 21452930]
69. Al-Ejeh F, Kumar R, Wiegmans A, Lakhani SR, Brown MP, Khanna KK. Harnessing the complexity of DNA-damage response pathways to improve cancer treatment outcomes. Oncogene. 2010; 29:6085–6098. [PubMed: 20818418]
70. Lassègue B, Griendling KK. NADPH oxidases: Functions and pathologies in the vasculature. Arterioscler Thromb Vasc Biol. 2010; 30:653–661. [PubMed: 19910640]
71. Lassègue B, San Martin A, Griendling KK. Biochemistry, physiology, and pathophysiology of NADPH oxidases in the cardiovascular system. Circ Res. 2012; 110:1364–1390. [PubMed: 22581922]
72. Nguyen Dinh Cat A, Montezano AC, Burger D, Touyz RM. Angiotensin II, NADPH oxidase, and redox signaling in the vasculature. Antioxid Redox Signal. 2013; 19:1110–1120. [PubMed: 22530599]
73. Schilder YDC, Heiss EH, Schachner D, Ziegler J, Reznicek G, Sorescu D, Dirsch VM. NADPH oxidases 1 and 4 mediate cellular senescence induced by resveratrol in human endothelial cells. Free Radic Biol Med. 2009; 46:1598–1606. [PubMed: 19328228]
74. Cevik MO, Katsuyama M, Kanda S, Kaneko T, Iwata K, Ibi M, Matsuno K, Kakehi T, Cui W, Sasaki M, Yabe-Nishimura C. The AP-1 site is essential for the promoter activity of NOX1/NADPH oxidase, a vascular superoxide-producing enzyme: Possible involvement of the ERK1/2-JunB pathway. Biochem Biophys Res Commun. 2008; 374:351–355. [PubMed: 18638447]
75. Al Ghouleh I, Sahoo S, Meijles DN, Amaral JH, de Jesus DS, Sembrat J, Rojas M, Goncharov DA, Goncharova EA, Pagano PJ. Endothelial Nox1 oxidase assembly in human pulmonary arterial hypertension; driver of Gremlin1-mediated proliferation. Clin Sci. 2017; 131:2019–2035. [PubMed: 28522681]
76. Li JM, Fan LM, George VT, Brooks G. Nox2 regulates endothelial cell cycle arrest and apoptosis via $p21^{cip1}$ and p53. Free Radic Biol Med. 2007; 43:976–986. [PubMed: 17697942]
77. Hotz MA, Gong J, Traganos F, Darzynkiewicz Z. Flow cytometric detection of apoptosis: Comparison of the assays of in situ DNA degradation and chromatin changes. Cytometry. 1994; 15:237–244. [PubMed: 8187583]
78. Meijles DN, Fan LM, Howlin BJ, Li JM. Molecular insights of $p47^{phox}$ phosphorylation dynamics in the regulation of NADPH oxidase activation and superoxide production. J Biol Chem. 2014; 289:22759–22770. [PubMed: 24970888]

79. Teng L, Fan LM, Meijles D, Li JM. Divergent effects of p47^{phox} phosphorylation at S303-4 or S379 on tumor necrosis factor-α signaling via TRAF4 and MAPK in endothelial cells. Arterioscler Thromb Vasc Biol. 2012; 32:1488–1496. [PubMed: 22460559]

80. Debacq-Chainiaux F, Erusalimsky JD, Campisi J, Toussaint O. Protocols to detect senescence-associated beta-galactosidase (SA-βgal) activity, a biomarker of senescent cells in culture and in vivo. Nat Protoc. 2009; 4:1798–1806. [PubMed: 20010931]

81. Meijles DN, Fan LM, Ghazaly MM, Howlin B, Krönke M, Brooks G, Li JM. p22^{phox} C242T single-nucleotide polymorphism inhibits inflammatory oxidative damage to endothelial cells and vessels. Circulation. 2016; 133:2391–2403. [PubMed: 27162237]

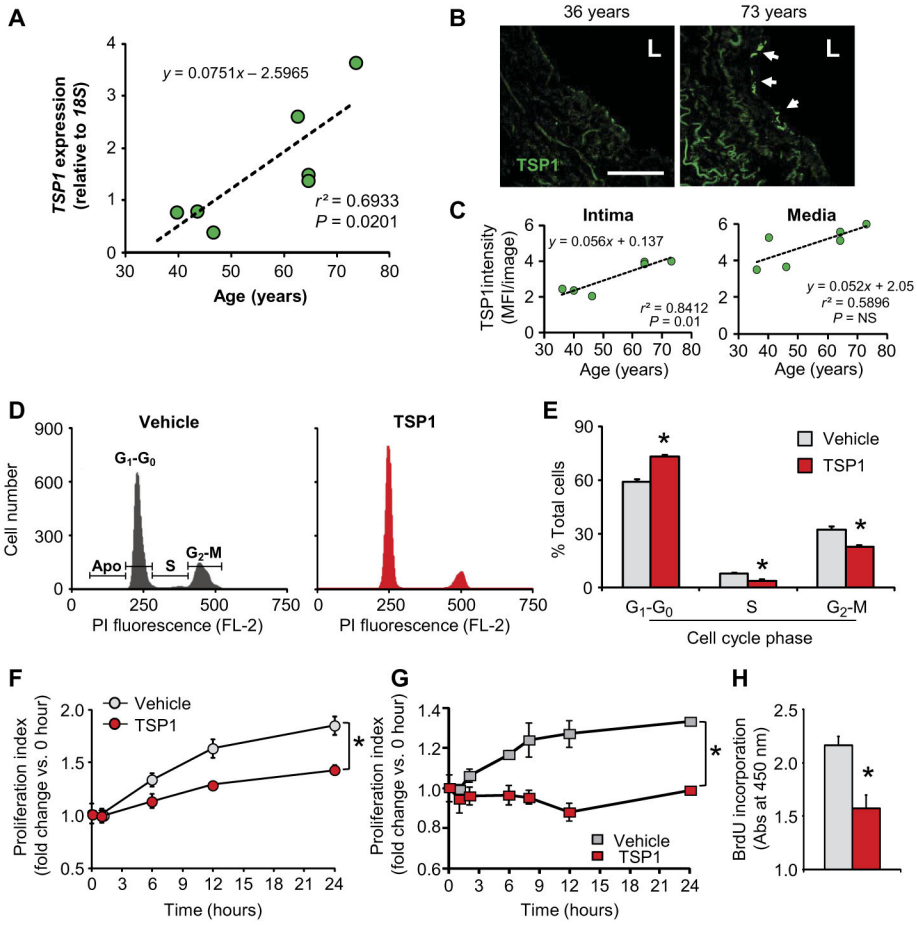

Fig. 1. TSP1 is increased in aging human lung vasculature and induces endothelial cell cycle arrest in vitro

Data for human tissue are shown in green; data for cell experiments are shown in red; data in gray are the corresponding controls. (**A**) Correlation of *TSP1* expression as quantified by quantitative reverse transcription polymerase chain reaction (qRT-PCR) with age in human lung homogenates ($n = 7$ subjects; r^2=0.69, $P = 0.02$). Data points are means of three replicates of the same sample. (**B**) Representative images of TSP1 protein abundance in the intimal and medial layer of human pulmonary arteries of a 73-year-old subject (right; arrows indicate intima) compared to an artery from a 36-year-old subject (left) as determined by immunofluorescence (IF). Scale bar, 100 μm. L, vascular lumen. (**C**) Quantitation of immunofluorescence images from six subjects ($n = 4$ samples each, 10 to 20 images per sample) is plotted as a linear regression; equation, r^2, and P values are as indicated. MFI, mean fluorescence intensity. (**D**) Cell cycle profile analysis of vehicle (left) and TSP1-challenged (right) HPAECs measured by propidium iodide (PI) labeling and fluorescence-activated cell sorting (FACS). FL-2, fluorescence channel 2. (**E**) Quantitative analysis of cell cycle phase distribution of HPAECs. Data are the means ± SEM of 20,000 events ($n = 4$ biological replicates per treatment group) expressed as percentage. *$P < 0.05$ for TSP1 challenge compared to vehicle control by Mann-Whitney test of each phase. (**F** and **G**) HPAEC proliferation in the presence or absence of TSP1, as measured by trypan blue

exclusion assay (F) and MTT assay (G). Data are means ± SEM ($n = 3$ biological replicates per treatment). $P < 0.001$ for TSP1 compared to vehicle control by repeated-measures analyses. (**H**) BrdU incorporation in HPAECs in the presence or absence of TSP1 at 24 hours. Data are means ± SEM ($n = 3$ biological replicates per treatment). *$P < 0.05$ for TSP1 challenge compared to vehicle control by Student's *t* test.

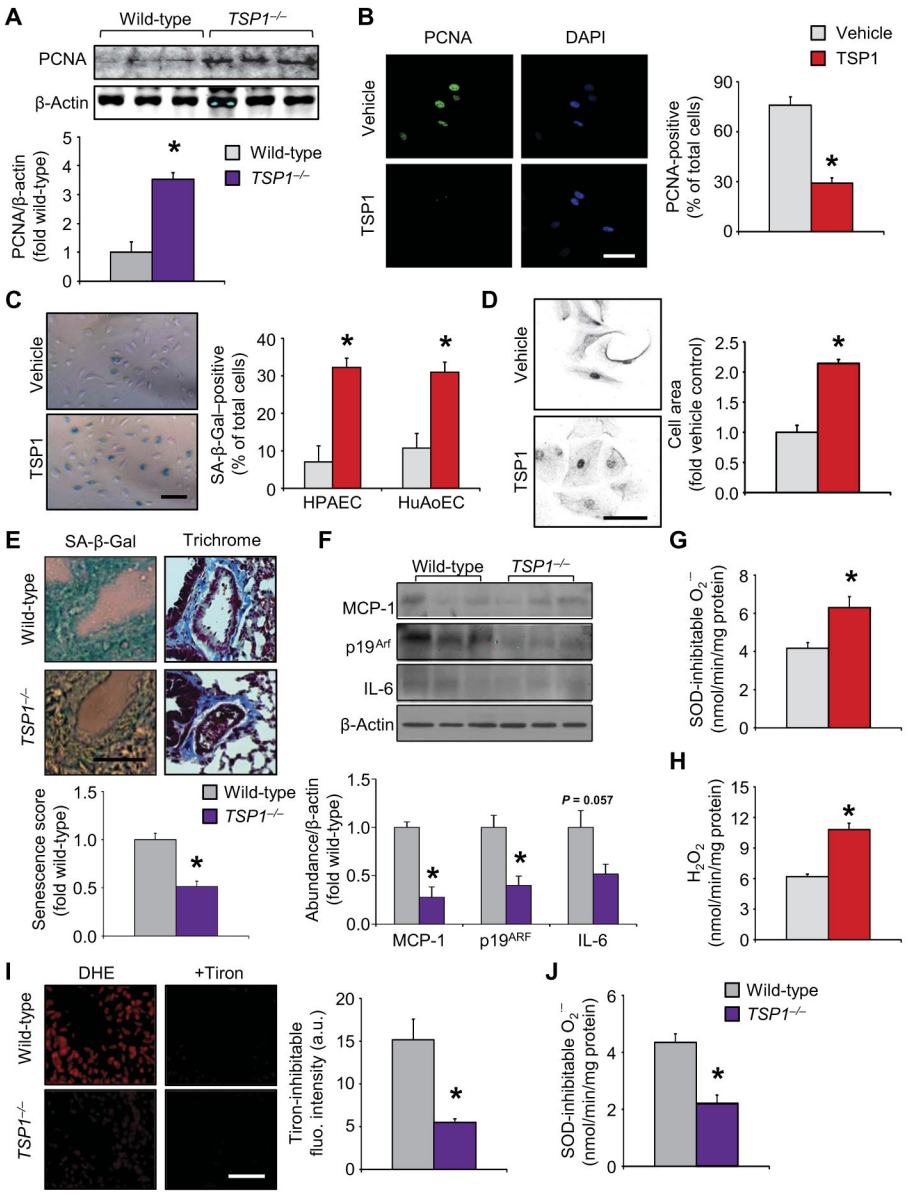

Fig. 2. TSP1 promotes cell and tissue senescence in vitro and oxidative stress in wild-type middle-aged mice

Data for *TSP1*$^{-/-}$ samples are plotted in purple; data for cell experiments are in red; data in gray represent the corresponding controls. (**A** and **B**) Abundance of the S phase–associated proliferation marker PCNA in middle-aged *TSP1*$^{-/-}$ mice (purple bar) compared to age-matched wild-type controls (gray bar) as analyzed by Western blotting (A) and in HPAECs exposed to TSP1 as analyzed by immunofluorescence (B). Data are means ± SEM [$n = 6$ animals per group (A); $n = 3$ cell populations per treatment, 10 to 20 images per immunodetection (scale bar, 20 μm)] (B); *$P < 0.05$ compared to wild-type or vehicle control by Student's t test. (**C** to **F**) Endothelial cell senescence as detected by SA-β-Gal labeling [C; HPAECs and human aortic endothelial cells (HuAoECs)] and increases in cell size (D; HPAECs). SA-β-Gal (E, left) and trichrome staining (E, right) were used on en face

tissue to visualize senescence, gross lung vessel morphology, and collagen deposition (blue) in middle-aged wild-type and *TSP1*$^{-/-}$ lungs. The abundance of SASP factors [MCP-1, p19^{Arf}, and interleukin-6 (IL-6)] was assessed by Western blotting in middle-aged *TSP1*$^{-/-}$ and age-matched wild-type controls (F; purple compared to gray bars). Data are means ± SEM (n = 3 independent experiments or n = 3 animals; 12 images per group). Scale bar, 100 μm. *P < 0.05 for TSP1 challenge compared to vehicle control or null compared to age-matched wild-type mice by Student's t test. (**G** and **H**) NADPH-driven $O_2^{\bullet-}$ (G; cytochrome c assay) and H_2O_2 (H; Amplex Red assay) production in HPAEC lysates. Data are means ± SEM (n = 4 biological replicates per treatment). *P < 0.05 compared to vehicle controls by Student's t test. (**I** and **J**) En face cell-permeant $O_2^{\bullet-}$ scavenger (Tiron)–inhibitable dihydroethidium (DHE)–ROS, as measured by fluorescence microscopy (I), and NADPH-driven homogenate $O_2^{\bullet-}$ production, as measured by cytochrome c reduction (J). Data are means ± SEM (n = 3 to 6 mice per group). Scale bar, 50 μm. *P < 0.05 compared to wild-type controls by Student's t test. a.u., arbitrary units.

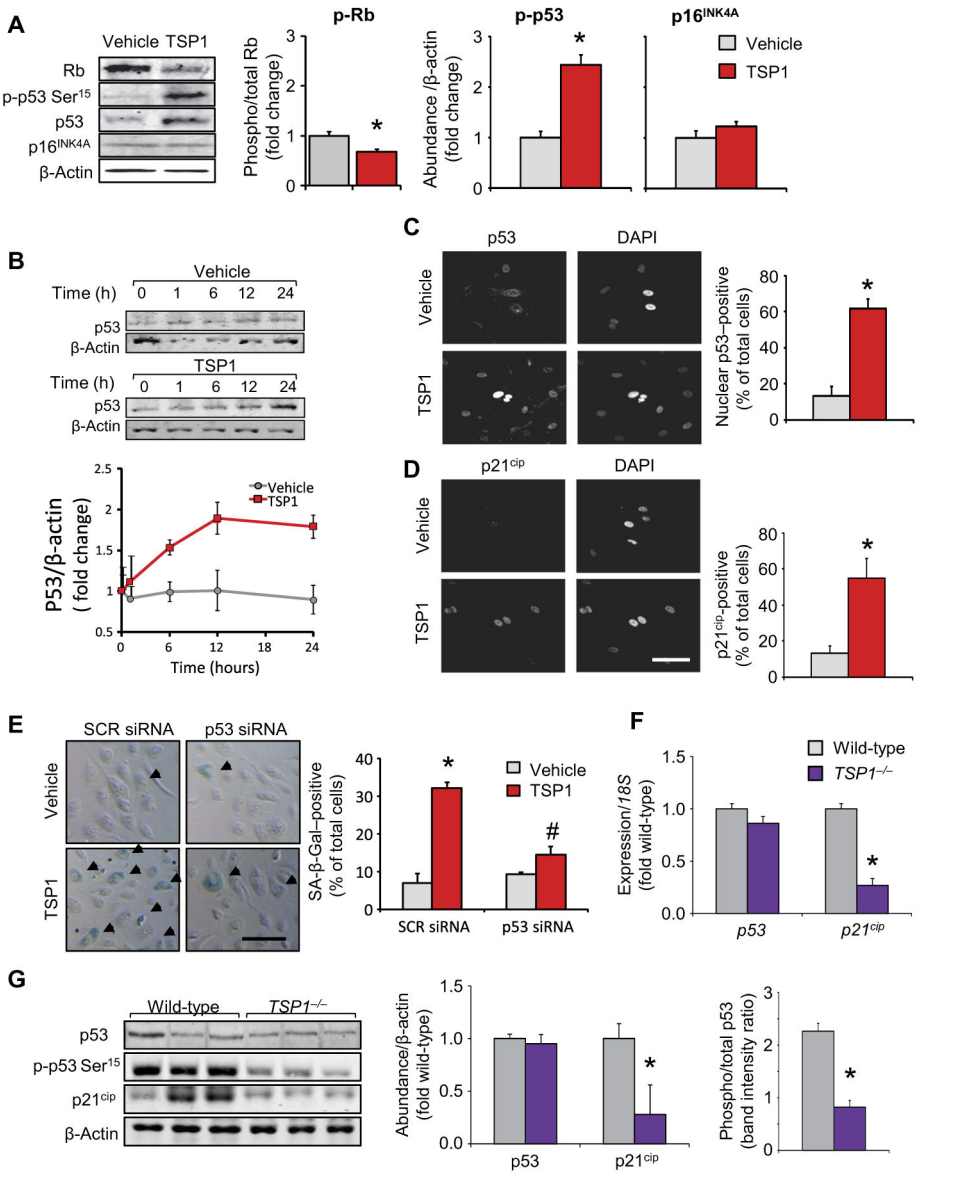

Fig. 3. TSP1 induces DDR-p53-p21^{cip} –mediated senescence.

Data for *TSP1*$^{-/-}$ samples are depicted in purple; data for cell experiments are in red; data in gray are the corresponding controls. (**A**) Abundance of Rb, total and phospho-Ser^{15} p53, and p16^{INK4A} after 24 hours of TSP1 challenge in HPAECs, as measured by Western blot. Data are means ± SEM (n = 3 biological replicates per treatment); *P < 0.05 compared to vehicle by Student's t test. (**B**) Time-dependent changes in p53 abundance in HPAECs stimulated with TSP1, as measured by Western blot. Graphical data are means ± SEM (n = 3 biological replicates per treatment), by repeated-measures analysis. (**C** and **D**) Activation of the p53 pathway, as assessed by nuclear localization of p53 (C), and p21^{cip} abundance (D), as measured by immunofluorescence, compared to vehicle controls. Data are means ± SEM (n = 3 biological replicates per treatment; 12 to 20 images per sample). Scale bar, 40 μm. *P <

0.05 for TSP1 challenge compared to vehicle control by Student's *t* test. DAPI, 4′,6-diamidino-2-phenylindole. (**E**) Effect of p53 knockdown by small interfering RNA (siRNA) on TSP1-induced senescence in HPAECs. Graphical data are means ± SEM ($n = 3$ biological replicates per treatment). Scale bar, 40 μm. $^{*}P < 0.05$ for TSP1 challenge compared to vehicle control; $^{\#}P < 0.05$ for p53 siRNA-TSP1 compared to scrambled siRNA (SCR)–TSP1 by one-way analysis of variance (ANOVA). (**F**) mRNA expression of *p53* and $p21^{cip}$ in middle-aged $TSP1^{-/-}$ animals. Data are means ± SEM ($n = 3$ individual animals for each group). $^{*}P < 0.05$ compared to wild-type by Student's *t* test. (**G**) Abundance of $p21^{cip}$ and total and phospho-p53 in middle-aged $TSP1^{-/-}$ lungs compared to wild-type, age-matched controls. Graphical data are means ± SEM ($n = 6$ animals per group). $^{*}P < 0.05$ for $TSP1^{-/-}$compared to wild-type by Student's *t* test.

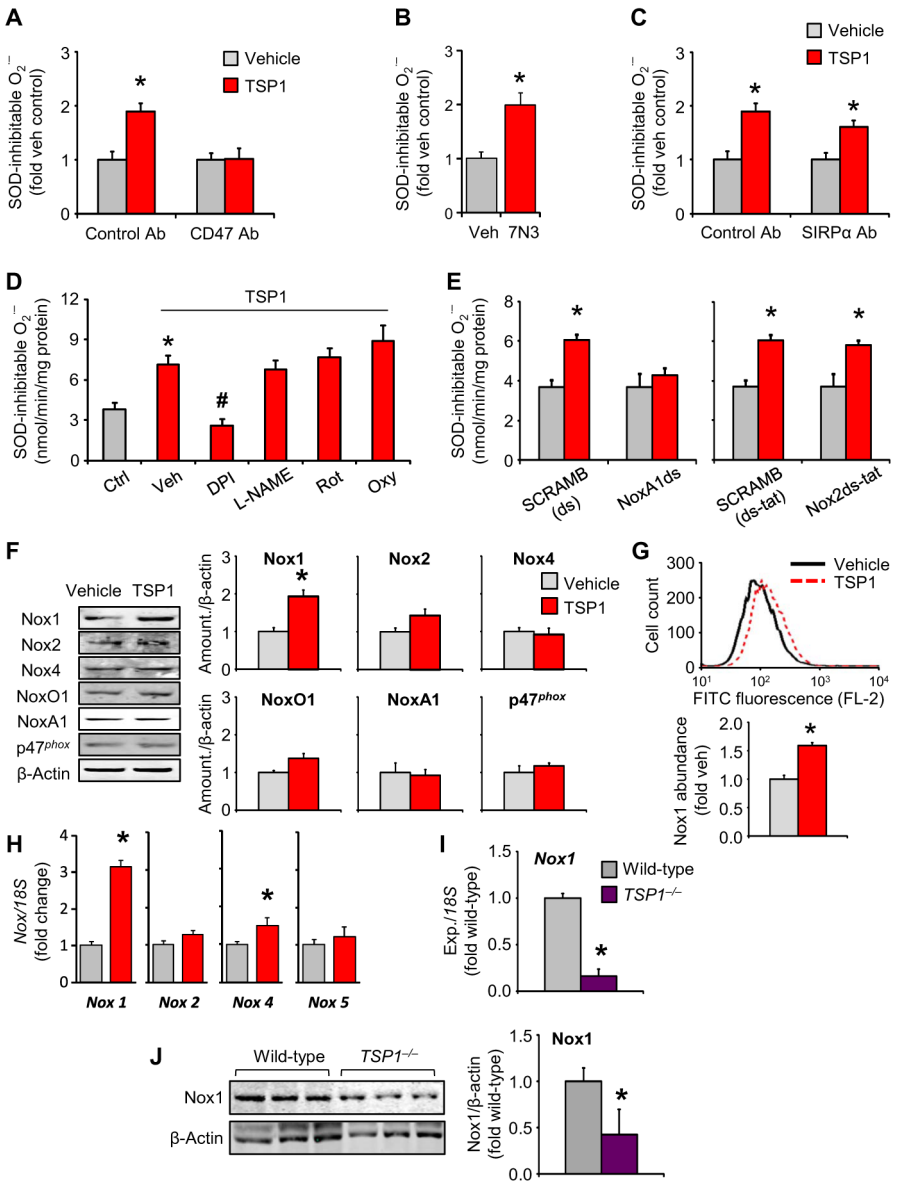

Fig. 4. TSP1 induces Nox1-dependent $O_2^{\bullet-}$ production in HPAECs through its receptor CD47

Data for *TSP1*$^{-/-}$ samples are shown in purple; data for cell experiments are shown in red; data in gray are the corresponding controls. (**A** and **B**) NADPH-driven $O_2^{\bullet-}$ production, as measured by cytochrome *c* reduction assay in HPAECs exposed to TSP1 in the presence or absence of a specific CD47 blocking antibody (Ab) (A) or the CD47-activating peptide 7N3 (B). Data are means ± SEM ($n = 3$ biological replicates per treatment). *$P < 0.05$ for TSP1 challenge compared to vehicle control (veh) by one-way ANOVA and *t* test, respectively. (**C**) TSP1-induced $O_2^{\bullet-}$ production in HPAECs exposed to a specific SIRPα blocking antibody. Data are means ± SEM ($n = 3$ biological replicates per treatment). *$P < 0.05$ for TSP1 challenge compared to vehicle control by one-way ANOVA. (**D**) TSP1-induced $O_2^{\bullet-}$ production in HPAECs exposed to inhibitors of eNOS (L-NAME), mitochondrial complex I [rotenone (Rot)], or xanthine oxidase [oxypurinol (Oxy)]. Data are means ± SEM ($n = 3$

biological replicates per treatment). *$P < 0.05$ for TSP1 challenge compared to inhibitor vehicle control; #$P < 0.05$ for inhibitor compared to TSP1-vehicle by Student's *t* test. (**E**) TSP1-induced $O_2^{\bullet-}$ production in HPAECs pretreated with the Nox1- and Nox2- specific inhibitory peptides, NoxA1ds (left) or Nox2ds-tat (right) or their respective scrambled controls (SCRAMB). Data are means ± SEM ($n = 3$ biological replicates per treatment). *$P < 0.05$ for TSP1 challenge compared to vehicle by one-way ANOVA. (**F** to **H**) Abundance in Nox family members in TSP1-challenged HPAECs, as assessed by Western blotting (F) and FACS (G). Graphical data are means ± SEM ($n = 3$ biological replicates per treatment). *$P < 0.05$ for TSP1 challenge compared to vehicle control by Student's *t* test. For qRT-PCR analysis (H), *$P < 0.05$ indicates significance for TSP1 challenge compared to vehicle control by Mann-Whitney test. (**I** and **J**) Nox1 abundance in lungs of *TSP1*$^{-/-}$ mice and wild-type age-matched controls at the mRNA level as demonstrated by RT-PCR (I) and at the protein level as demonstrated by immunoblotting (J). Graphical data are means ± SEM ($n = 3$ to 6 animals per group). *$P < 0.05$ for *TSP1*$^{-/-}$ compared to wild-type control by Student's *t* test.

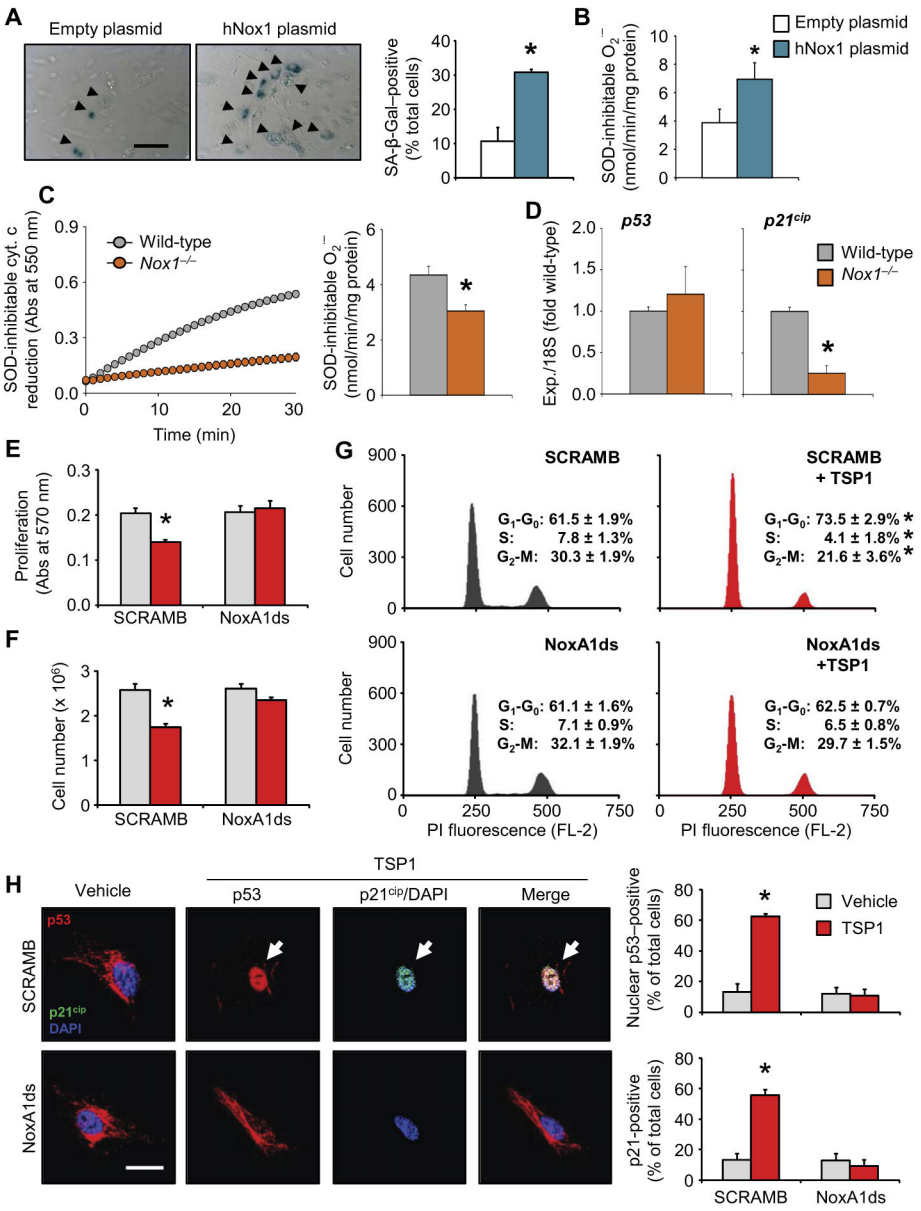

Fig. 5. Nox1 as a potential therapeutic target to inhibit matricellular-mediated endothelial senescence

Data for $Nox1^{OE}$ are shown in blue; data for $Nox1^{-/-}$ samples are shown in orange; data for cell experiments are shown in red; data in gray are the corresponding controls. (**A** and **B**) Effect of human $Nox1^{OE}$ on SA-β-Gal staining and $O_2^{\bullet-}$ production. Graphical data are means ± SEM ($n = 3$ biological replicates per treatment). Scale bar, 40 μm. *$P < 0.05$ for Nox1 plasmid compared to empty plasmid control by Student's t test. (**C**) NADPH-driven $O_2^{\bullet-}$ production, as measured by cytochrome c reduction assay in middle-aged wild-type and *Nox1*$^{-/-}$ mouse lungs. Left: Representative cytochrome c kinetic curve. Right: Quantification of $O_2^{\bullet-}$ production. Bar graphs are means ± SEM ($n = 6$ mice per group). *$P < 0.05$ compared to wild-type by Student's t test. (**D**) mRNA expression of *p53* and *p21*^{cip} in wild-type and *Nox1*$^{-/-}$ mouse lungs. Data are the means ± SEM ($n = 3$ mice per group); *P

< 0.05 compared to wild type by Student's *t* test. (**E** to **G**) Effect of Nox1 inhibition (using NoxA1ds) on TSP1-induced cell cycle arrest in HPAECs, as measured by MTT assay (E), trypan blue exclusion assay (F), and cell cycle profile analysis (G). Graphical data are means ± SEM (n = 3 to 4 biological replicates per treatment). *P < 0.05 for TSP1 challenge compared to scrambled vehicle control (SCRAMB) by one-way ANOVA. (**H**) Activation of p53 (red), as assessed by nuclear localization (DAPI-labeled, blue) and $p21^{cip}$ immunofluorescence (green) in HPAECs challenged with TSP1 in the presence or absence of the Nox1 inhibitor NoxA1ds. Graphical data are means ± SEM (n = 3 biological replicates per treatment, 12 to 20 images per group). Scale bar, 50 μm. *P < 0.05 for TSP1 challenge compared to scrambled vehicle control by one-way ANOVA.

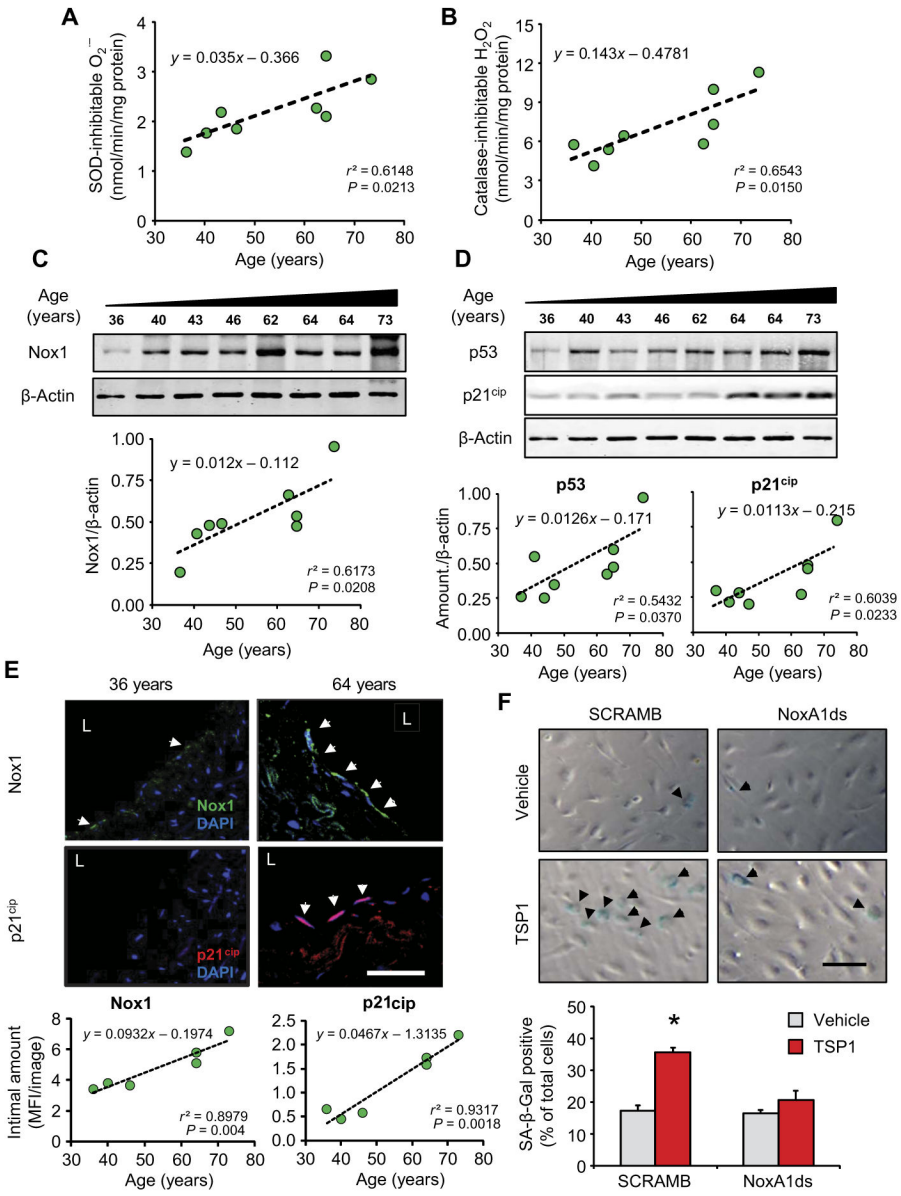

Fig. 6. Potential clinical relevance of Nox1-mediated endothelial senescence in human pulmonary vascular tissue

Data points for human tissue are shown in green; data for cell experiments are shown in red; data in gray are the corresponding controls. Data for (**A**) to (**E**) are plotted as linear regression ($n = 8$ samples); equation, r^2, and P values are indicated in the corresponding graph. (A and B) Correlation between NADPH-driven $O_2^{\bullet-}$ production, as measured by cytochrome *c* reduction (A), or H_2O_2 production, as measured by Amplex Red fluorescence (B), and age in human lung homogenates. (C and D) Abundance of Nox1 (C) and p53 and $p21^{cip}$ (D), as measured by Western blot of total homogenates of aging human lung. (**E**) Intimal immunofluorescence for Nox1 (top, green) and $p21^{cip}$ (bottom, red) in aged human lung sections. Scale bar, 50 μm. Graphs show linear regression analyses. (**F**) HPAEC senescence induced by TSP1 in the presence or absence of NoxA1ds, as measured by SA-β-

Gal staining. Graphical data are means ± SEM (n = 3 biological replicates per treatment). Scale bar, 40 μm. *P < 0.05 for TSP1 challenge compared to scrambled vehicle control by Student's t test.

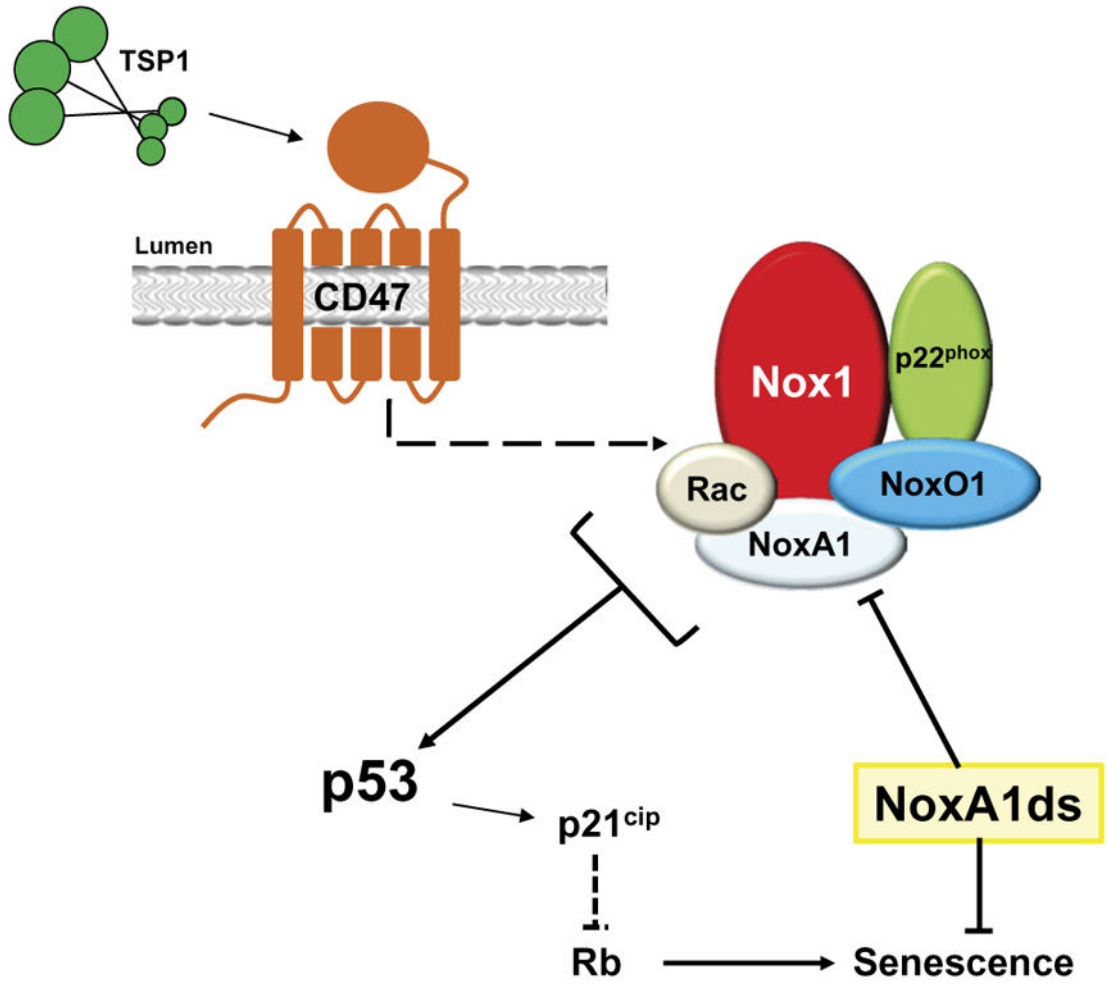

Fig. 7. A signaling model for TSP1-induced senescence

Upon binding to CD47, TSP1 activates the Nox1 complex, which generates robust and sustained accumulation of ROS. In turn, this triggers committed senescence through a pathway involving p53-p21^{cip}–induced DNA damage response and decreased Rb phosphorylation. This pathway can be disrupted using the selective Nox1 inhibitor NoxA1ds.